HHS Public Access

Author manuscript

Neuroimage. Author manuscript; available in PMC 2021 October 01.

Published in final edited form as:

Neuroimage. 2021 October 01; 239: 118267. doi:10.1016/j.neuroimage.2021.118267.

Investigation of the association between cerebral iron content and myelin content in normative aging using quantitative magnetic resonance neuroimaging

Nikkita Khattar[a], **Curtis Triebswetter**[a], **Matthew Kiely**[a], **Luigi Ferrucci**[b], **Susan M. Resnick**[c], **Richard G. Spencer**[a], **Mustapha Bouhrara**[a,*]

[a]Laboratory of Clinical Investigation, National Institute on Aging, National Institutes of Health, Baltimore, 21224 MD, United States

[b]Translational Gerontology Branch, National Institute on Aging, National Institutes of Health, Baltimore, 21224 MD, United States

[c]Laboratory of Behavioral Neuroscience, National Institute on Aging, National Institutes of Health, Baltimore, 21224 MD, United States

Abstract

Myelin loss and iron accumulation are cardinal features of aging and various neurodegenerative diseases. Oligodendrocytes incorporate iron as a metabolic substrate for myelin synthesis and maintenance. An emerging hypothesis in Alzheimer's disease research suggests that myelin breakdown releases substantial stores of iron that may accumulate, leading to further myelin breakdown and neurodegeneration. We assessed associations between iron content and myelin content in critical brain regions using quantitative magnetic resonance imaging (MRI) on a cohort of cognitively unimpaired adults ranging in age from 21 to 94 years. We measured whole-brain myelin water fraction (MWF), a surrogate of myelin content, using multicomponent relaxometry, and whole-brain iron content using susceptibility weighted imaging in all individuals. MWF was negatively associated with iron content in most brain regions evaluated indicating that lower myelin content corresponds to higher iron content. Moreover, iron content was significantly higher with advanced age in most structures, with men exhibiting a trend towards higher iron content as compared to women. Finally, relationship between MWF and age, in all brain regions investigated, suggests that brain myelination continues until middle age, followed by degeneration at older ages. This work establishes a foundation for further investigations of the etiology and sequelae of myelin breakdown and iron accumulation in neurodegeneration and may lead to new imaging markers for disease progression and treatment.

*Corresponding author at: Magnetic Resonance Physics of Aging and Dementia Unit, National Institute on Aging, National Institutes of Health, Intramural Research Program, BRC 05C-222, 251 Bayview Boulevard, Baltimore, MD 21224, USA. bouhraram@mail.nih.gov (M. Bouhrara).

Authors contribution

MB: experimental design, MB, NK: data acquisition, NK, CT, MK: data preprocessing, NK, CT, MK, MB: data analysis, NK, CT, MK, RGS, LF, SMR, MB: data interpretation, NK, MB: paper drafting, NK, CT, MK, RGS, LF, SMR, MB: paper editing.

Supplementary materials

Supplementary material associated with this article can be found, in the online version, at doi:10.1016/j.neuroimage.2021.118267.

Keywords

Iron; Myelin; Quantitative MRI; Aging

1. Introduction

Iron is involved in several biological processes that are paramount for normal neurologic function, including oxygen transportation, mito-chondrial respiration, oxidative phosphorylation, and synthesis of neurotransmitters. In addition, it is an essential cofactor for enzymatic activity related to myelin production and maintenance. Oligodendrocytes, the cells that produce myelin, are the main iron-containing cells of the CNS and incorporate iron as a substrate for myelin production (Todorich et al., 2009; Möller et al., 2019). The importance of iron for myelin production has been demonstrated through observations of demyelination accompanying decreased dietary iron (Ortiz et al., 2004; Hare et al., 2013; Stankiewicz et al., 2014), and the fact that in animal models, injection of ferritin, the main iron storage protein, into white matter promotes oligodendrogenesis (Schonberg et al., 2012; Schonberg and McTigue, 2009). However, studies have also shown that iron may accumulate in several brain regions with aging. If iron homeostasis is not maintained, excess iron has the potential to catalyze free radical reactions; this promotes oxidative damage of brain tissue, ultimately potentiating impairments in cognition and behavior (Ghadery et al., 2015; Emerit et al., 2001; Hallgren and Sourander, 1958). Indeed, it has been shown that dysregulation of iron homeostasis is a critical feature of various neurodegenerative diseases, including Alzheimer's disease (AD), Parkinson's disease (PD), and Huntington's disease (Lane et al., 2018; Mills et al., 2010).

An emerging hypothesis in AD research, put forward by Bartzokis *et al.*, suggests that myelin breakdown and degeneration of oligodendrocytes release substantial stores of iron that, absent appropriate clearance, may accumulate in the brain leading to further myelin and tissue damage including neurodegeneration (Möller et al., 2019; Hallgren and Sourander, 1958; Bartzokis, 2004; Bartzokis, 2011; Bartzokis et al., 2003; Bartzokis et al., 2004; G Bartzokis et al., 2007; Bartzokis et al., 2000). This paradigm is increasingly supported by preclinical and clinical studies demonstrating substantial iron release from damaged myelin sheets or oligodendrocytes (Heidari et al., 2016; SE Nasrabady et al., 2018). Further, in a recent magnetic resonance imaging (MRI) study of animals and humans, it has been shown that mutations within the hemochromatosis gene, which results in increased iron overload, lead to white matter degradation; this was interpreted as a direct consequence of demyelination (Meadowcroft et al., 2016). Moreover, Hametner and colleagues, in their immunohistochemistry study of iron distribution and expression of iron-related proteins in human brain tissue affected by multiple sclerosis (MS) (Hametner et al., 2013), have shown that in active MS lesions, iron was released from dying oligodendrocytes resulting in extracellular accumulation of iron which leads to cell degeneration (Haider, 2015). Further, Steiger and colleagues have demonstrated that ventral striatum iron accumulation is linked to demyelination and impairments in declarative memory in healthy young and elderly participants (Steiger et al., 2016). Notwithstanding these findings, the association

between myelin breakdown and cerebral iron accumulation in normal aging requires further investigation.

MRI provides a unique tool to quantify, *in-vivo,* iron and myelin contents. Ferritin and neuromelanin polymer pigments are the main reservoirs of iron in the human brain. Inside these complexes, iron forms aggregates that lead, in the presence of an external magnetic field, to the creation of strong magnetic susceptibility inhomogeneities and consequent local field distortions. These distortions are detectable at submillimeter resolution using various susceptibility-sensitive MRI techniques, such as susceptibility weighted imaging (SWI) (EM Haacke et al., 2009). In SWI, iron depositions exhibit negative regional phase, resulting in decreased image intensity in the vicinity of iron (Wang et al., 2012; Pfefferbaum et al., 2009; Xu et al., 2008; Haacke et al., 2004; Haacke et al., 2007). SWI, and its advanced version, namely, quantitative susceptibility mapping (QSM), have been shown to be sensitive techniques for investigating age-dependent iron deposition in normal aging, neurodegeneration, and dementia (Wang et al., 2012; Pfefferbaum et al., 2009; Xu et al., 2008; C Liu et al., 2015; Sehgal et al., 2005; EM Haacke et al., 2009; Harder et al., 2008; van der Weijden et al., 2019; Acosta-Cabronero et al., 2016; Betts et al., 2016; Keuken et al., 2017; Zhang et al., 2018; Bilgic et al., 2012; Lin et al., 2015; Killiany et al., 2020; Li et al., 2021; Darki et al., 2016; Chen et al., 2021). Furthermore, MRI mapping of myelin water fraction (MWF), a proxy of myelin content, provides important insights for understanding brain maturation and neurodegeneration (Bouhrara and Spencer, 2016; MacKay and Laule, 2016; Whittall et al., 1997; Does, 2018; Alonso-Ortiz et al., 2015; Piredda et al., 2021; MacKay et al., 1994; Vavasour et al., 2006). Advanced analysis methods based on multicomponent relaxometry have been introduced to improve both sensitivity and specificity of MR-based myelin quantification (Bouhrara and Spencer, 2016; MacKay and Laule, 2016; Whittall et al., 1997; Does, 2018; Alonso-Ortiz et al., 2015; Piredda et al., 2021; Jones et al., 2003; Prasloski et al., 2012; Bonny et al., 2020; M Bouhrara et al., 2021; Bouhrara et al., 2015); these methods have been extensively applied to characterize cerebral demyelinating diseases and neurodevelopment (MacKay and Laule, 2016; Borich et al., 2013; Laule et al., 2006; Sirrs et al., 2007; Kolind et al., 2012; Kolind et al., 2015; Dean et al., 2017; Dean et al., 2014; Dean et al., 2016; Deoni et al., 2012; M Bouhrara et al., 2020; M Bouhrara et al., 2020; Bouhrara et al., 2018; M Bouhrara et al., 2020; Qian et al., 2020; Dvorak et al., 2021; Papadaki et al., 2019). Using MWF and QSM, Yao and colleagues have shown an association between focal iron accumulation and myelin loss in patients with chronic MS lesions (Yao et al., 2018). Using the same MRI techniques, Pu and colleagues have shown a negative correlation between myelin and iron content in the basal ganglia and in the connecting white matter fibers in macaques (Pu et al., 2020). These findings provide compelling support for the unique sensitivity and specificity of MRI-based approaches to quantify, *in-vivo*, myelin and iron, and shed light on the intimate relationship between myelin breakdown and iron deposition. We refer the reader to an excellent review by Möller and colleagues of the clinical role of multiparametric MR imaging in quantifying local iron and myelin content as emerging important biomarkers for white matter and cerebral tissue integrity (Möller et al., 2019).

In this work, we investigate the regional associations between iron content and myelin content in normative aging of the human brain using advanced quantitative

MR neuroimaging. For mapping myelin, we use the Bayesian Monte-Carlo analysis of multicomponent driven equilibrium steady-state observation of T_1 and T_2 (BMC-mcDESPOT) method, developed in our laboratory and applied extensively (Bouhrara and Spencer, 2016; M Bouhrara et al., 2021; M Bouhrara et al., 2020; M Bouhrara et al., 2020; Bouhrara et al., 2018; M Bouhrara et al., 2020; Qian et al., 2020; Bouhrara et al., 2016; Bouhrara and Spencer, 2015; Bouhrara and Spencer, 2017; M Bouhrara et al., 2021; M Bouhrara et al., 2017; M Bouhrara et al., 2017). Iron content is measured using our implementation of high-resolution SWI. Our study is conducted on a cohort of 92 well-characterized healthy adults over an age range of 21 to 94 years, with the main goal of developing further insights into the biochemical mechanisms of iron deposition in the human brain.

2. Material & methods

2.1. Participants

Participants were drawn from the Baltimore Longitudinal Study of Aging (BLSA) (Shock, 1985; Ferrucci, 2008), and the Genetic and Epigenetic Signatures of Translational Aging Laboratory Testing (GESTALT) study. The study populations, experimental design, and measurement protocols of the BLSA have been previously reported (Shock, 1985; Ferrucci, 2008). The BLSA is a longitudinal cohort study funded and conducted by the NIA Intramural Research Program (IRP). Established in 1958, the BLSA enrolls community-dwelling adults with no major chronic conditions or functional impairments at enrollment. The GESTALT study is also a study of healthy volunteers, initiated in 2015, and funded and conducted by the NIA IRP. The goal of the BLSA and GESTALT studies is to evaluate multiple biomarkers related to aging. We note that the inclusion and exclusion criteria for these two studies are essentially identical. Participants underwent testing at the NIA's clinical research unit and were excluded if they had metallic implants, or major neurologic or medical disorders. All participants underwent a Mini Mental State Examination (MMSE). Seven participants with cognitive impairment were excluded from the analysis. The final cohort consisted of 92 cognitively unimpaired volunteers (mean ± standard deviation MMSE = 28.6 ± 1.7) ranging in age from 21 to 94 years (54.3 ± 22.3 years) of which 50 were men (56.4 ± 23.8 years) and 42 were women (51.8 ± 20.3 years). Age ($p > .05$) and MMSE ($p > .05$) did not differ significantly between men and women. The number of participants per age-decade was: 12 (7 women) within 20–29 years, 15 (5 women) within 30–39 years, 26 (15 women) within 40–49 years, 4 (1 woman) within 50–59 years, 4 (3 women) within 60–69 years, 12 (5 women) within 70– 79 years, 16 (6 women) within 80–89 years, and 3 (0 woman) within 90–99 years. Experimental procedures were performed in compliance with our local Institutional Review Board, and participants provided written informed consent.

2.2. MR imaging

MRI scans were performed on a 3T whole body Philips MRI system (Achieva, Best, The Netherlands) using the internal quadrature body coil for transmission and an eight-channel phased-array head coil for reception. For each participant, the imaging protocol was as follow:

- BMC-mcDESPOT for MWF mapping (Bouhrara and Spencer, 2016; Bouhrara et al., 2016; Bouhrara and Spencer, 2015; Bouhrara and Spencer, 2017): 3D spoiled gradient recalled echo (SPGR) images were acquired with flip angles (FAs) of [2 4 6 8 10 12 14 16 18 20]°, echo time (TE) of 1.37 ms, repetition time (TR) of 5 ms, bandwidth (BW) of 1478 Hz/pixel, and acquisition time of ~5 min. In addition, 3D balanced steady state free precession (bSSFP) images were acquired with FAs of [2 4 7 11 16 24 32 40 50 60]°, TE of 2.8 ms, TR of 5.8 ms, BW of 1918 Hz/pixel, and acquisition time of ~6 min. The bSSFP images were acquired with radiofrequency (RF) excitation pulse phase increments of 0 or π in order to account for off-resonance effects (Deoni, 2011). All SPGR and bSSFP images were acquired with an acquisition matrix of 150 × 130 × 94, voxel size of 1.6 mm × 1.6 mm × 1.6 mm, and 94 slices. TEs and TRs were set to the minimum values to improve detection of the signal from the rapidly relaxing component of myelin water and to reduce the total acquisition time, while the FA values were based on suggested values from literature as well as on our extensive simulation analyses conducted previously to define the set of FAs required to maximize accuracy and precision in derived MWF values (Bouhrara and Spencer, 2016; Bouhrara et al., 2016; Bouhrara and Spencer, 2015; Bouhrara and Spencer, 2017; Deoni, 2011; Deoni et al., 2013; Deoni et al., 2008). Further, we used the double-angle method (DAM) to correct for excitation RF inhomogeneity (Stollberger and Wach, 1996). For that, two fast spin-echo images were acquired with FAs of 45° and 90°, TE of 102 ms, TR of 3000 ms, acquisition voxel size of 2.6 mm × 2.6 mm × 4 mm, 38 slices, and acquisition time of ~4 min. All images were acquired with a field-of-view (FoV) of 240 mm × 208 mm × 150 mm. The total acquisition time was ~21 min.
- SWI for iron content mapping (Wang et al., 2012; Pfefferbaum et al., 2009; Xu et al., 2008; C Liu et al., 2015): 3D single-echo SW image was acquired using a gradient-echo sequence with flow compensation, FoV of 240 mm x 240 mm x 185 mm, voxel size of 0.64 mm × 0.64 mm × 0.64 mm, 290 slices, EPI-factor of 15, TR of 47 ms, TE of 27 ms, and 2 signal averages. The total acquisition time was ~3 min. Both magnitude and phase images were saved.

All images were acquired with a SENSE factor of 2 and reconstructed to a voxel size of 1 mm × 1 mm × 1 mm. We emphasize that all MRI studies and ancillary measurements were performed with the same MRI system, running the same pulse sequences, at the same facility, and directed by the same principal investigator for both BLSA and GESTALT participants.

2.3. Image processing

After thorough visual inspection of data quality for each participant, the scalp, ventricles, and other nonparenchymal regions within the images were eliminated using the BET tool as implemented in the FSL software (Smith, 2002). For each participant, using FSL (Jenkinson et al., 2012), all SPGR, bSSFP, or DAM images were linearly registered to the SPGR image obtained at FA of 8° and the respective derived transformation matrices were then applied to the original SPGR, bSSFP, or DAM images. Then, a whole-brain MWF map

was generated using BMC-mcDESPOT from these co-registered SPGR, bSSFP, and DAM datasets (Bouhrara and Spencer, 2016; Bouhrara et al., 2018; Bouhrara and Spencer, 2015; Bouhrara and Spencer, 2017), while a whole-brain SWI phase map was generated using the phase and magnitude SWI dataset (Wang et al., 2012; Pfefferbaum et al., 2009; Xu et al., 2008; C Liu et al., 2015) (Fig. 1). Using the FSL software, the averaged SPGR image over FAs was nonlinearly registered to the MNI atlas, and the computed transformation matrix was then applied to the corresponding MWF map. Similarly, the magnitude SWI image was nonlinearly registered to the MNI atlas, and the computed transformation matrix was then applied to the corresponding SWI phase map (Fig. 1).

Twenty white matter (WM) and deep gray matter (DGM) regions of interest (ROIs) within the cerebrum were defined from the MNI atlas. Twelve WM regions were defined from the Johns Hopkins University (JHU) ICM-DTI-81 atlas encompassing the entire brain, the frontal, parietal, temporal and occipital lobes, as well as the corpus callosum, internal capsules, cerebellum, forceps, fronto-occipital fasciculus and longitudinal fasciculus, while eight DGM regions were defined encompassing the hippocampus, amygdala, caudate, thalamus, putamen, red nucleus, insula, substantia nigra and globus pallidus (Fig. 3), corresponding to regions previously identified in studies of cerebral iron or myelin content, as the focus of our investigation (Steiger et al., 2016; Wang et al., 2012; Pfefferbaum et al., 2009; Xu et al., 2008; M Bouhrara et al., 2020; Dvorak et al., 2021; Aquino et al., 2009; Persson et al., 2015; Faizy et al., 2018; Faizy et al., 2020; Uddin et al., 2019; J Zhang et al., 2015; Arshad et al., 2016). Mean SWI phase and MWF values were calculated for each ROI; these regional measures are provided in the Supplementary Material. In the SWI phase maps, regions with strong magnetic susceptibility or high iron concentration are surrounded by bright areas or rims exhibiting abnormally high phase values (Pfefferbaum et al., 2009; Xu et al., 2008). Therefore, to avoid introducing bias into derived mean SWI phase values, voxels belonging to these regions were excluded, as per conventional practice (Pfefferbaum et al., 2009; Xu et al., 2008), through application of a signal intensity threshold (Fig. 2). Furthermore, all ROIs were eroded to avoid partial volume bias from adjacent structures or from the edges of the brain which are affected by strong air-tissue magnetic susceptibility interfaces.

2.4. Statistical analyses

To investigate the effects of age and sex on SWI phase, multilinear regression was applied using the mean SWI phase within each ROI as the dependent variable and sex and age as the independent variables. In all cases, the interaction term between sex and age was found to be non-significant and was therefore omitted from the final model.

A similar analysis was performed to assess the effects of age and sex on MWF, with mean MWF within each ROI as the dependent variable and sex, age, and age^2 as the independent variables, after mean age centering. The inclusion of age^2 as an independent variable is based on our and others' recent observations that MWF follows a quadratic relationship with age (M Bouhrara et al., 2020; M Bouhrara et al., 2020; Qian et al., 2020; Dvorak et al., 2021; Arshad et al., 2016). In all cases, interaction terms between sex and age or sex and age^2 were found to be non-significant and were therefore omitted from the final model.

Finally, as the main focus of this work, we investigated the association between SWI phase and MWF using multilinear regression, with the mean SWI phase within each ROI as the dependent variable and the MWF within the ROI, age, and sex as the independent variables.

For all analyses, the threshold for statistical significance was $p < .05$ after correction for multiple ROI comparisons using the false discovery rate (FDR) method (Benjamini, 2010; Benjamini and Hochberg, 1995). All calculations were performed with MATLAB (MathWorks, Natick, MA, USA).

3. Results

3.1. Age and sex effects on iron and myelin contents

Fig. 4 shows SWI phase and MWF maps for representative participants of three different ages. Results are shown for two representative axial slices covering the main brain structures investigated. Visual inspection indicates lower SWI phase values at higher ages, while MWF exhibited a quadratic, inverted U-shape, association with age; this is attributed to the process of myelination from youth through middle age, followed by demyelination afterward. Furthermore, we note that different regions exhibit different patterns of association between SWI phase or MWF and age, as expected.

Fig. 5 shows quantitative results for mean SWI phase values from all participants as a function of age for the indicated 20 WM and DGM cerebral regions. These results show lower mean SWI phase, that is, higher iron content, with age in most examined ROIs ($p < .05$, FDR corrected), except the red nucleus, the globus pallidus, and the substantia nigra which showed no trend with age (Table 1). The best-fit curves indicate that while the fundamental linear decreasing relationship between mean SWI phase and age was consistent across most of the ROIs, there was, as expected, some regional variation. The steepest negative slopes in SWI phase with age were found in the caudate, putamen, and internal capsule regions, while the smallest slopes were found in the temporal and parietal lobes. In addition, the lowest mean SWI phase values across age, that is, the highest iron content, were found in the DGM ROIs, namely, the caudate, thalamus, putamen, red nucleus, insula, substantia nigra and globus pallidus, while the highest SWI phase values, that is, the lowest iron content values, were found in the WM ROIs, especially the temporal lobe and cerebellum. Finally, the effect of sex on SWI phase was not significant in any of the cerebral regions investigated (Table 1), although in most ROIs, men exhibited nonsignificant trends toward lower SWI phase values, that is, greater iron content, than women (Table 1).

Fig. 6 shows quantitative results for MWF values from all participants as a function of age for the 20 indicated WM and DGM cerebral regions. Unlike mean SWI phase, MWF *vs.* age exhibits nonlinear trends increasing until middle age and decreasing afterward in most ROIs examined. The best-fit curves indicate that while the fundamental inverted U-shaped relationship between MWF and age was consistent across all ROIs, this relationship displayed regional variation. Significant age effects on MWF were observed in all the brain regions evaluated, except the caudate, putamen, substantia nigra, amygdala and hippocampus ROIs (Table 2), with reduced MWF with advancing age. The steepest decline of MWF with age was found in the corpus callosum while the slowest decline was seen

in the internal capsules. Similarly, the quadratic effect of age, age^{2,} was significant in all brain structures evaluated (Table 2). Furthermore, as expected, the highest MWF values were found in the WM ROIs, with the DGM ROIs exhibiting overall lower MWF values. Finally, the effect of sex on MWF was not significant in any of the cerebral regions investigated (Table 2). In most ROIs, men exhibited nonsignificant trends towards higher MWF values, that is, greater myelin content, than women (Table 2).

3.2. Association between iron content and myelin content

Fig. 7 shows the results of the regressions of SWI phase with MWF, after adjusting for age and sex, for the 20 indicated WM and DGM cerebral regions studied. As seen, lower MWF, that is, lower myelin content, corresponds to lower SWI phase values, that is, higher iron content, in most ROIs examined, with the best-fit curves displaying regional variation. Our statistical analysis, presented in Table 3, shows that the relationship between MWF and SWI phase was significant ($p < .05$) or close to significance ($p < .1$) in all brain regions, except in the occipital lobes, cerebellum, caudate, insula, putamen, and fronto-occipital fasciculus ROIs. In addition, the steepest positive slopes in SWI phase with MWF were found in the amygdala and hippocampus, while the smallest slopes were found in the cerebellum, putamen, and occipital lobes (Table 3).

4. Discussion

Using advanced MR methodology for myelin and iron content quantification, we demonstrate significant associations between iron content or myelin content with age in a cohort of healthy volunteers. Further, our results indicate significant negative associations between iron content and myelin content; these associations were statistically significant in various critical brain regions, even after adjusting for age and sex. While these results do not confirm a causal link between iron deposition and myelin breakdown, they provide further evidence of a potential link between iron neurochemistry and myelin integrity in aging adults.

Our results indicate linear associations between iron content and age in all WM and DGM regions investigated (Table 1, Fig. 5) and confirm the significant effects of age on brain iron levels (Hallgren and Sourander, 1958; Wang et al., 2012; Pfefferbaum et al., 2009; Xu et al., 2008; Acosta-Cabronero et al., 2016; Persson et al., 2015; Ramos et al., 2014; Daugherty and Raz, 2015; Haacke et al., 2010). These findings are consistent with previous reports, indicating overall trends of lower SWI phase values, that is, higher iron content, with age in several WM and DGM regions (Wang et al., 2012; Pfefferbaum et al., 2009; Xu et al., 2008). Our results show that the rates of iron deposition varied across cerebral structures, in agreement with several previous *in-vivo* and post-mortem studies (Hallgren and Sourander, 1958; Pfefferbaum et al., 2009; Xu et al., 2008; Aquino et al., 2009) (Table 1). Indeed, we found that age-differences in iron concentration in the globus pallidus, red nucleus, putamen, and caudate were not significant (Xu et al., 2008; Acosta-Cabronero et al., 2016; Aquino et al., 2009). Studies have also suggested that iron accumulation in these structures is nonlinear over time, with iron levels approaching a distinct plateau in middle age (Hallgren and Sourander, 1958; Xu et al., 2008; Aquino et al., 2009). Finally, our data showed that there

were no sex related differences in iron content in any of the regions studied, although men exhibited nonsignificant trends of higher iron content than women (Table 1); this agrees with previous observations (Xu et al., 2008; Persson et al., 2015; G Bartzokis et al., 2007). However, the literature regarding sex differences in iron content remains sparse (Xu et al., 2008), with larger cohort studies required for further definition of this potential effect.

Our results indicate a quadratic association between MWF and age in all cerebral regions investigated (Table 2, Fig. 6). These results are consistent with our and previous reports, on larger cohorts of cognitively unimpaired participants, indicating an inverted U-shape trend of MWF values with age in several white matter regions (M Bouhrara et al., 2020; Dvorak et al., 2021; Papadaki et al., 2019; Arshad et al., 2016). This quadratic association between myelin and age is attributed to the process of progressive myelination from youth through middle age, followed by demyelination in later years (Arshad et al., 2016; Bartzokis et al., 2010); this pattern is in agreement with postmortem observations (Peters, 2002; Tang et al., 1997) and with several studies based on myelin-sensitive MRI methods such as diffusion tensor imaging and relaxation rates (Bartzokis et al., 2010; Okubo et al., 2017; Westlye et al., 2010; Yeatman et al., 2014; Slater et al., 2019).

As expected, our results show variation among brain regions. The DGM structures exhibited the steepest slope in the relationship between iron content and myelination (Table 3, Fig. 7). Postmortem and *in vivo* studies have shown large amounts of iron in the basal ganglia in cognitively unimpaired individuals (Möller et al., 2019; Hallgren and Sourander, 1958; Bartzokis et al., 2000; Wang et al., 2012; Pfefferbaum et al., 2009; Xu et al., 2008; Ramos et al., 2014; G Bartzokis et al., 2007; Griffiths and Crossman, 1993; Bartzokis et al., 1994; Ogg et al., 1999; Loeffler et al., 1995; Ward et al., 2014). Indeed, iron is stored in the ferritin protein which is present in high concentration in the basal ganglia (Griffiths and Crossman, 1993; Griffiths et al., 1999). However, our results must be interpreted with caution. It has been shown that diffusion of iron into the extracellular space may decrease the relaxation times of the unbound water pool, leading to an artificial overestimation of MWF values with increasing iron content (Birkl et al., 2019); this could explain the opposite trends seen in the substantia nigra, caudate and red nucleus (Fig. 5), which are known to exhibit the highest iron concentrations in the human brain. However, in spite of this potential effect, our results in fact show lower MWF with higher iron content. This indicates that a physiologic association of demyelination with increased iron content dominates this potential source of error in many of the ROIs examined. However, overestimation of MWF due to iron may be responsible for rendering the association nonsignificant in other ROIs despite consistent trends in the direction of this association. Ongoing studies incorporating additional subjects, longitudinal follow up, and histological measures will provide further insight into these phenomena.

The relationship between local iron content and myelination may provide important insight into their roles in neurodegenerative diseases, especially given the vulnerability of oligodendrocyte metabolism to iron neurotoxicity. A powerful argument has emerged incorporating impaired myelin homeostasis as a central phenomenon in the pathophysiology of Alzheimer's disease (AD). This concept, introduced by Bartzokis and colleagues (Bartzokis, 2004; Bartzokis, 2011; Bartzokis et al., 2004; G Bartzokis et al., 2007), suggests

that myelin breakdown releases iron which promotes the development of amyloid plaques, which in turn destroy additional myelin. However, myelin and the oligodendrocytes that produce it are vulnerable to the accumulation of amyloid-β protein, tau protein, or iron (Dean et al., 2017; Bradl and Lassmann, 2010; SE Nasrabady et al., 2018; Desai et al., 2010). Consequent loss of oligodendrocytes or impairment of their metabolic synthetic function in the setting of AD, and possibly other dementias, may therefore result in focal myelination deficits. These deficits may in turn serve as the pathophysiologic basis of decreased interregional connectivity in the central nervous system (CNS) and subsequent decreased cognitive ability, as well as other deficits in CNS function. This myelin paradigm is supported by clinical MRI studies showing decreases in myelin content in the setting of AD and mild cognitive impairment (MCI) (Bouhrara et al., 2018; Carmeli et al., 2013; van der Flier et al., 2002; Arfanakis et al., 2007; Kabani et al., 2002; Gold et al., 2012; Haris et al., 2009). Furthermore, growing evidence indicates decreases in myelin production with decreased dietary iron (Ortiz et al., 2004; Hare et al., 2013; Stankiewicz et al., 2014). All these considerations led us to the plausible hypothesis of an association between iron content and myelin content. These studies, our previous report providing evidence of myelin loss in MCI and dementia (Bouhrara et al., 2018) and our current findings motivate our ongoing studies of the relationship between iron accumulation and myelin loss in MCI and dementia, including longitudinal studies designed to evaluate the temporal relationship between demyelination and iron deposition. If confirmed, this would establish a therapeutic target for AD prevention, namely, maintenance of iron homeostasis through pharmacological treatments, such as iron chelation or dietary interventions. In addition, correlations with symptomatology would serve to establish MWF and iron quantifications as biomarkers for the progression of AD.

Although our work examines a relatively large cohort and uses advanced methodology, several limitations remain. Our dataset is cross-sectional, so that the iron and myelin associations observed here require further validation through longitudinal studies, which may provide insights regarding the causality of these associations. Such work, motivated by the present results, is underway. We also note that it was not feasible to obtain optimal uniform sampling across all age intervals in this sample of participants. In fact, the number of subjects included between 50 and 70 years is much lower as compared to the other age decades. This may also influence the overall interpretability of myelination or iron, as well as their associations, during the process of aging (Fjell et al., 2010). Nevertheless, we obtained a meaningful sample size across the age range of our study. Moreover, other metals such as manganese or copper can affect the measured MR signal. However, the concentration of these metals in the brain, under normal conditions, is extremely low so that the local phase distortions, as depicted in the SWI phase maps, are mainly due to iron. Moreover, our SWI analysis was based on a single-echo acquisition (Wang et al., 2012; Pfefferbaum et al., 2009; Xu et al., 2008). Further studies of the association between myelin and iron contents using more quantitative and advanced techniques, such as QSM for iron quantification, are needed (Langkammer et al., 2012; C Liu et al., 2015; Wang and Liu, 2015). Furthermore, although the susceptibility-weighted contrast in the brain is driven primarily by iron (Haacke et al., 2005; Yao et al., 2009; Hametner et al., 2018), myelin, whose elevated content in lipids and proteins renders its sheaths diamagnetic, may

contribute to susceptibility contrast (Kor et al., 2019; Lee et al., 2012; Li et al., 2011); this may introduce some bias in derived SWI phase values. Histological studies are required to further explore this potential confounder. Moreover, as indicated above, it has been shown that diffusion of iron into the extracellular space may shorten the corresponding transverse relaxation time leading to an artificial overestimation of MWF values (Birkl et al., 2019; Drayer et al., 1986). Further *ex-vivo* or histological experiments are required to unambiguously elucidate the origin of this observation (Kirilina et al., 2020). Nevertheless, we note that since iron could lead to increases in derived MWF values while myelin sheets could lead to lower derived SWI phase values, a positive association between iron and MWF would be expected. In this case, these effects would be antagonist to our observation of regional negative associations between iron and MWF; this provides further support to our observation despite the aforementioned competing effects. Interestingly, positive or no associations between iron and MWF were observed in a few deep gray matter regions (DGM), including the red nucleus, substantia nigra and caudate; these structures exhibit very high iron concentrations. We conjecture that these positive associations found in these DGM regions are likely driven by a strong bias in derived MWF values due to a high iron concentration. In addition, fiber orientation effects may represent another factor that could bias iron and MWF estimates (Kor et al., 2019; Lee et al., 2010; Liu, 2010; Birkl et al., 2021). Another source of bias in derived MWF values is myelin debris from damaged myelin sheets. Indeed, myelin debris can be interpreted as intact myelin in multicomponent MRI analysis (Webb et al., 2003; McCreary et al., 2009; Kozlowski et al., 2008). Moreover, contamination due to partial volume issues may have been introduced in the calculated MWF or SWI values. To mitigate this contamination, all ROIs were eroded followed by careful visual inspections. Nevertheless, some partial volume effects could have persisted, especially in small structures including the deep gray matter ROIs. In addition, age-related tissue atrophy could lead to nonoptimal image registration, potentially introducing some bias in derived parameters values. Nevertheless, our visual inspection indicates that age-related tissue atrophy was limited to a very few participants belonging to the oldest age decade of our cohort. Finally, several physiological and experimental parameters could bias MWF determination. These include, but are not limited to, exchange between water pools (West et al., 2019; Kalantari et al., 2011; Myint and Ishima, 2009), magnetization transfer between free water protons and macromolecules (West et al., 2019; J Zhang et al., 2015), iron content (Birkl et al., 2019), internal gradients (Washburn et al., 2008; Seland et al., 2004), and differential signal attenuation due to water diffusion in underlying compartments (Ziener et al., 2010; Carney et al., 1991; Le Bihan et al., 1989), which are not considered in either the BMC-mcDESPOT formalism or the other MWF measurement methods available. The importance of these effects in a particular experiment will depend both on the specifics of the sample or subject under investigation and on the details of the pulse sequence, including the selection of parameters such as TE, TR, FA, RF pulse characteristics and gradient durations and amplitudes (Does, 2018; Alonso-Ortiz et al., 2015; Dvorak et al., 2021; Levesque et al., 2010; Lazari and Lipp, 2021; Bouhrara and Bonny, 2012). However, it must be emphasized that multi-spin echo-based MRI sequences, namely the Carr–Purcell–Meiboom–Gill sequence or its accelerated version, the gradient and spin echo sequence, remain the reference methods for MWF mapping (MacKay and Laule, 2016; Alonso-Ortiz et al., 2015; Piredda et al., 2021; Dvorak et al., 2021; Lazari and Lipp, 2021; Lee et al., 2021;

Heath et al., 2018). This is likely due to the availability of these imaging sequences on most preclinical and clinical MRI systems, the simplicity of the signal model, and the extensive histological validation conducted over the last two decades (Laule et al., 2006; Laule et al., 2008).

In this study, examining the association between local myelination and iron accumulation in the human cerebrum, we showed that higher iron content is associated with lower myelin content across a wide age range of cognitively normal subjects.

Supplementary Material

Refer to Web version on PubMed Central for supplementary material.

Acknowledgments

This work was supported by the Intramural Research Program of the National Institute on Aging of the National Institutes of Health. We gratefully acknowledge Christopher M. Bergeron, Jan Bergeron, Denise Melvin, and Linda Zukley for their assistance with data acquisition, and participant recruitment and logistics.

References

Acosta-Cabronero J, Betts MJ, Cardenas-Blanco A, Yang S, Nestor PJ, 2016. In VivoMRI mapping of brain iron deposition across the adult lifespan. J. Neurosci. 36 (2), 364–374. [PubMed: 26758829]

Alonso-Ortiz E, Levesque IR, Pike GB, 2015. MRI-based myelin water imaging: a technical review. Magn. Reson. Med. 73 (1), 70–81. [PubMed: 24604728]

Aquino D, Bizzi A, Grisoli M, Garavaglia B, Bruzzone MG, Nardocci N, et al., 2009. Age-related iron deposition in the basal ganglia: quantitative analysis in healthy subjects. Radiology252 (1), 165–172. [PubMed: 19561255]

Arfanakis K, Gui M, Tamhane AA, Carew JD, 2007. Investigating the Medial Temporal Lobe in Alzheimer's Disease and Mild Cognitive Impairment, with Turboprop Diffusion Tensor Imaging, MRI-volumetry, and T 2-relaxometry. Brain Imaging Behav. 1 (1), 11–21.

Arshad M, Stanley JA, Raz N, 2016. Adult age differences in subcortical myelin content are consistent with protracted myelination and unrelated to diffusion tensor imaging indices. Neuroimage143, 26–39. [PubMed: 27561713]

Bartzokis G, Cummings JL, Sultzer D, Henderson VW, Nuechterlein KH, Mintz J, 2003. White matter structural integrity in healthy aging adults and patients with Alzheimer disease: a magnetic resonance imaging study. Arch. Neurol. 60 (3), 393–398. [PubMed: 12633151]

Bartzokis G, Lu PH, Mintz J, 2004. Quantifying age-related myelin breakdown with MRI: novel therapeutic targets for preventing cognitive decline and Alzheimer's disease. J. Alzheimer's Dis. 6 (6 Suppl), S53–S59. [PubMed: 15665415]

Bartzokis G, Lu PH, Mintz J, 2007a. Human brain myelination and amyloid beta deposition in Alzheimer's disease. Alzheimer's Dementia3 (2), 122–125.

Bartzokis G, Lu PH, Tingus K, Mendez MF, Richard A, Peters DG, et al., 2010. Lifespan trajectory of myelin integrity and maximum motor speed. Neurobiol. Aging31 (9), 1554–1562. [PubMed: 18926601]

Bartzokis G, Mintz J, Sultzer D, Marx P, Herzberg JS, Phelan CK, et al., 1994. In vivo MR evaluation of age-related increases in brain iron. AJNR Am. J. Neuroradiol. 15 (6), 1129–1138. [PubMed: 8073983]

Bartzokis G, Sultzer D, Cummings J, et al., 2000. In vivo evaluation of brain iron in alzheimer disease using magnetic resonance imaging. Arch. Gen. Psychiatry57 (1), 47–53. [PubMed: 10632232]

Bartzokis G, Tishler TA, Lu PH, Villablanca P, Altshuler LL, Carter M, et al., 2007b. Brain ferritin iron may influence age- and gender-related risks of neurodegeneration. Neurobiol. Aging28 (3), 414–423. [PubMed: 16563566]

Bartzokis G, 2004. Age-related myelin breakdown: a developmental model of cognitive decline and Alzheimer's disease. Neurobiol. Aging25 (1), 5–18 author reply 49–62. [PubMed: 14675724]

Bartzokis G, 2011. Alzheimer's disease as homeostatic responses to age-related myelin breakdown. Neurobiol. Aging32 (8), 1341–1371. [PubMed: 19775776]

Benjamini Y, Hochberg Y, 1995. Controlling the false discovery rate: a practical and powerful approach to multiple testing. J. R. Statistic. Soc. Ser. B (Methodological)57 (1), 289–300.

Benjamini Y, 2010. Discovering the false discovery rate. J. R. Statistic. Soc. Ser. B (Statistic. Methodol.)72 (4), 405–416.

Betts MJ, Acosta-Cabronero J, Cardenas-Blanco A, Nestor PJ, Düzel E, 2016. High--resolution characterisation of the aging brain using simultaneous quantitative susceptibility mapping (QSM) and R2∗ measurements at 7T. Neuroimage138, 43–63. [PubMed: 27181761]

Bilgic B, Pfefferbaum A, Rohlfing T, Sullivan EV, Adalsteinsson E, 2012. MRI estimates of brain iron concentration in normal aging using quantitative susceptibility mapping. Neuroimage59 (3), 2625–2635. [PubMed: 21925274]

Birkl C, Birkl-Toeglhofer AM, Endmayr V, Hoftberger R, Kasprian G, Krebs C, et al., 2019. The influence of brain iron on myelin water imaging. Neuroimage199, 545–552. [PubMed: 31108214]

Birkl C, Doucette J, Fan M, Hernández-Torres E, Rauscher A, 2021. Myelin water imaging depends on white matter fiber orientation in the human brain. Magn. Reson. Med. 85 (4), 2221–2231. [PubMed: 33017486]

Bonny J−M, Traore A, Bouhrara M, Spencer RG, Pages G, 2020. Parsimonious discretization for characterizing multi-exponential decay in magnetic resonance. NMR Biomed e4366.

Borich MR, MacKay AL, Vavasour IM, Rauscher A, Boyd LA, 2013. Evaluation of white matter myelin water fraction in chronic stroke. NeuroImage2, 569–580. [PubMed: 24179808]

Bouhrara M, Alisch J, Nikkita N, Kim R, Rejimon A, Cortina L, et al., 2020a. Association of cerebral blood flow with myelin content in cognitively unimpaired adults. BMJ Neurol. Open2, e000053.

Bouhrara M, Bonny JM, 2012. B(1) mapping with selective pulses. Magn. Reson. Med. 68 (5), 1472–1480. [PubMed: 22246956]

Bouhrara M, Cortina LE, Rejimon AC, Khattar N, Bergeron C, Bergeron J, et al., 2020b. Quantitative age-dependent differences in human brainstem myelination assessed using high-resolution magnetic resonance mapping. Neuroimage206, 116307.

Bouhrara M, Khattar N, Elango P, Resnick SM, Ferrucci L, Spencer RG, 2021a. Evidence of association between obesity and lower cerebral myelin content in cognitively unimpaired adults. Int. J. Obes. 45 (4), 850–859.

Bouhrara M, Kim RW, Khattar N, Qian W, Bergeron CM, Melvin D, et al., 2021. Age-related estimates of aggregate g-ratio of white matter structures assessed using quantitative magnetic resonance neuroimaging. Human Brain Mapping42, 2362–2373. [PubMed: 33595168]

Bouhrara M, Reiter D, Bergeron C, Zukley L, Ferrucci L, Resnick S, et al., 2018. Evidence of demyelination in mild cognitive impairment and dementia using a direct and specific magnetic resonance imaging measure of myelin content. Alzheimer's & Dementia14 (8), 998–1004.

Bouhrara M, Reiter DA, Bergeron CM, Zukley LM, Resnick SM, Studenski S, et al., 2017a. Demyelination in Mild Cognitive Impairment. ISMRM, Honolulu, HI, USA.

Bouhrara M, Reiter DA, Celik H, Fishbein KW, Kijowski R, Spencer RG, 2016. Analysis of mcDESPOT- and CPMG-derived parameter estimates for two-component nonexchanging systems. Magn. Reson. Med. 75 (6), 2406–2420. [PubMed: 26140371]

Bouhrara M, Reiter DA, Sexton KW, Bergeron CM, Zukley LM, Spencer RG, 2017b. Clinical high-resolution mapping of the proteoglycan-bound water fraction in articular cartilage of the human knee joint. Magn. Reson. Imaging43, 1–5. [PubMed: 28645697]

Bouhrara M, Reiter DA, Spencer RG, 2015. Bayesian analysis of transverse signal decay with application to human brain. Magn. Reson. Med. 74 (3), 785–802. [PubMed: 25242062]

Bouhrara M, Rejimon AC, Cortina LE, Khattar N, Bergeron CM, Ferrucci L, et al., 2020c. Adult brain aging investigated using BMC-mcDESPOT based myelin water fraction imaging. Neurobiol. Aging85, 131–139. [PubMed: 31735379]

Bouhrara M, Spencer RG, 2015. Incorporation of nonzero echo times in the SPGR and bSSFP signal models used in mcDESPOT. Magn. Reson. Med. 74 (5), 1227–1235. [PubMed: 26407635]

Bouhrara M, Spencer RG, 2016. Improved determination of the myelin water fraction in human brain using magnetic resonance imaging through Bayesian analysis of mcDESPOT. Neuroimage127, 456–471. [PubMed: 26499810]

Bouhrara M, Spencer RG, 2017. Rapid simultaneous high-resolution mapping of myelin water fraction and relaxation times in human brain using BMC-mcDESPOT. Neuroimage147, 800–811. [PubMed: 27729276]

Bradl M, Lassmann H, 2010. Oligodendrocytes: biology and pathology. Acta Neuropathol. 119 (1), 37–53. [PubMed: 19847447]

Carmeli C, Donati A, Antille V, Viceic D, Ghika J, von Gunten A, et al., 2013. Demyelination in mild cognitive impairment suggests progression path to Alzheimer's disease. PLoS ONE8 (8), e72759.

Carney CE, Wong ST, Patz S, 1991. Analytical solution and verification of diffusion effect in SSFP. Magn. Reson. Med. 19 (2), 240–246. [PubMed: 1881310]

Chen L, Soldan A, Oishi K, Faria A, Zhu Y, Albert M, et al., 2021. Quantitative susceptibility mapping of brain iron and -amyloid in MRI and PET relating to cognitive performance in cognitively normal older adults. Radiology298 (2), 353–362. [PubMed: 33231528]

Darki F, Nemmi F, Möller A, Sitnikov R, Klingberg T, 2016. Quantitative susceptibility mapping of striatum in children and adults, and its association with working memory performance. Neuroimage136, 208–214. [PubMed: 27132546]

Daugherty AM, Raz N, 2015. Appraising the role of iron in brain aging and cognition: promises and limitations of MRI methods. Neuropsychol. Rev. 25 (3), 272–287. [PubMed: 26248580]

Dean DC 3rd, Hurley SA, Kecskemeti SR, O'Grady JP, Canda C, Davenport–Sis NJ, et al., 2017. Association of amyloid pathology with myelin alteration in preclinical Alzheimer disease. JAMA Neurol. 74 (1), 41–49. [PubMed: 27842175]

Dean DC Iii, Jerskey BA, Chen K, et al., 2014. Brain differences in infants at differential genetic risk for late-onset alzheimer disease: a cross-sectional imaging study. JAMA Neurol. 71 (1), 11–22. [PubMed: 24276092]

Dean III DC, Sojkova J, Hurley S, Kecskemeti S, Okonkwo O, Bendlin BB, et al., 2016. Alterations of myelin content in Parkinson's disease: a cross-sectional neuroimaging study. PLoS ONE11 (10), e0163774. [PubMed: 27706215]

Deoni SC, Matthews L, Kolind SH, 2013. One component? Two components? Three? The effect of including a nonexchanging "free" water component in multicomponent driven equilibrium single pulse observation of T1 and T2. Magn. Reson. Med. 70 (1), 147–154. [PubMed: 22915316]

Deoni SC, Rutt BK, Arun T, Pierpaoli C, Jones DK, 2008. Gleaning multicomponent T1 and T2 information from steady-state imaging data. Magn. Reson. Med. 60 (6), 1372–1387. [PubMed: 19025904]

Deoni SC, 2011. Correction of main and transmit magnetic field (B0 and B1) inhomogeneity effects in multicomponent-driven equilibrium single-pulse observation of T1 and T2. Magn. Reson. Med. 65 (4), 1021–1035. [PubMed: 21413066]

Deoni SCL, Dean DC, O'Muircheartaigh J, Dirks H, Jerskey BA, 2012. Investigating white matter development in infancy and early childhood using myelin water faction and relaxation time mapping. Neuroimage63 (3), 1038–1053. [PubMed: 22884937]

Desai MK, Mastrangelo MA, Ryan DA, Sudol KL, Narrow WC, Bowers WJ, 2010. Early Oligodendrocyte/Myelin Pathology in Alzheimer's Disease Mice Constitutes a Novel Therapeutic Target. Am. J. Pathol. 177 (3), 1422–1435. [PubMed: 20696774]

Does MD, 2018. Inferring brain tissue composition and microstructure via MR relaxometry. Neuroimage182, 136–148. [PubMed: 29305163]

Drayer B, Burger P, Darwin R, Riederer S, Herfkens R, Johnson GA, 1986. MRI of brain iron. Am. J. Roentgenol. 147 (1), 103–110. [PubMed: 3487201]

Dvorak AV, Swift-LaPointe T, Vavasour IM, Lee LE, Abel S, Russell-Schulz B, et al., 2021. An atlas for human brain myelin content throughout the adult life span. Sci. Rep. 11 (1), 269. [PubMed: 33431990]

Emerit J, Beaumont C, Trivin F, 2001. Iron metabolism, free radicals, and oxidative injury. Biomed. Pharmacother. 55 (6), 333–339. [PubMed: 11478586]

Faizy TD, Kumar D, Broocks G, Thaler C, Flottmann F, Leischner H, et al., 2018. Age-Related measurements of the myelin water fraction derived from 3D multi-echo GRASE reflect myelin content of the cerebral white matter. Sci Rep8 (1), 14991. [PubMed: 30301904]

Faizy TD, Thaler C, Broocks G, Flottmann F, Leischner H, Kniep H, et al., 2020. The myelin water fraction serves as a marker for Age-related myelin alterations in the cerebral white matter – a multiparametric MRI aging study. Front Neurosci14 (136).

Ferrucci L, 2008. The Baltimore Longitudinal Study of Aging (BLSA): a 50-year-long journey and plans for the future. J. Gerontol. Series A63 (12), 1416–1419.

Fjell AM, Walhovd KB, Westlye LT, Ostby Y, Tamnes CK, Jernigan TL, et al., 2010. When does brain aging accelerate? Dangers of quadratic fits in cross-sectional studies. Neuroimage50 (4), 1376–1383. [PubMed: 20109562]

Ghadery C, Pirpamer L, Hofer E, Langkammer C, Petrovic K, Loitfelder M, et al., 2015. R2* mapping for brain iron: associations with cognition in normal aging. Neurobiol. Aging36 (2), 925–932. [PubMed: 25443291]

Gold BT, Jiang Y, Powell DK, Smith CD, 2012. Multimodal imaging evidence for axonal and myelin deterioration in amnestic mild cognitive impairment. J. Alzheimer's Dis. 31 (Suppl 3), S19–S31. [PubMed: 22460327]

Griffiths PD, Crossman AR, 1993. Distribution of iron in the basal ganglia and neocortex in postmortem tissue in Parkinson's disease and Alzheimer's disease. Dementia4 (2), 61–65. [PubMed: 8358514]

Griffiths PD, Dobson BR, Jones GR, Clarke DT, 1999. Iron in the basal ganglia in Parkinson's disease: an in vitro study using extended X-ray absorption fine structure and cryo-electron microscopy. Brain122 (4), 667–673. [PubMed: 10219780]

Haacke EM, Ayaz M, Khan A, Manova ES, Krishnamurthy B, Gollapalli L, et al., 2007. Establishing a baseline phase behavior in magnetic resonance imaging to determine normal vs. abnormal iron content in the brain. J. Magnetic Resonance Imaging: JMRI26 (2), 256–264.

Haacke EM, Cheng NY, House MJ, Liu Q, Neelavalli J, Ogg RJ, et al., 2005. Imaging iron stores in the brain using magnetic resonance imaging. Magn. Reson. Imaging23 (1), 1–25. [PubMed: 15733784]

Haacke EM, Makki M, Ge Y, Maheshwari M, Sehgal V, Hu J, et al., 2009a. Characterizing iron deposition in multiple sclerosis lesions using susceptibility weighted imaging. J. Magnet. Resonance Imag. 29 (3), 537–544.

Haacke EM, Miao Y, Liu M, Habib CA, Katkuri Y, Liu T, et al., 2010. Correlation of putative iron content as represented by changes in R2* and phase with age in deep gray matter of healthy adults. J. Magnet. Resonance Imag. 32 (3), 561–576.

Haacke EM, Mittal S, Wu Z, Neelavalli J, Cheng Y−CN, 2009b. Susceptibility-weighted imaging: technical aspects and clinical applications, part 1. Am. J. Neuroradiol. 30 (1), 19–30. [PubMed: 19039041]

Haacke EM, Xu Y, Cheng YC, Reichenbach JR, 2004. Susceptibility weighted imaging (SWI). Magn. Reson. Med52 (3), 612–618. [PubMed: 15334582]

Haider L, 2015. Inflammation, Iron, Energy Failure, and Oxidative Stress in the Pathogenesis of Multiple Sclerosis. Oxid Med Cell Longev2015, 725370.

Hallgren B, Sourander P, 1958. The effect of age on the non-haemin iron in the human brain. J. Neurochem. 3 (1), 41–51. [PubMed: 13611557]

Hametner S, Endmayr V, Deistung A, Palmrich P, Prihoda M, Haimburger E, et al., 2018. The influence of brain iron and myelin on magnetic susceptibility and effective transverse relaxation - A biochemical and histological validation study. Neuroimage179, 117–133. [PubMed: 29890327]

Hametner S, Wimmer I, Haider L, Pfeifenbring S, Brück W, Lassmann H, 2013. Iron and neurodegeneration in the multiple sclerosis brain. Ann. Neurol. 74 (6), 848–861. [PubMed: 23868451]

Harder SL, Hopp KM, Ward H, Neglio H, Gitlin J, Kido D, 2008. Mineralization of the deep gray matter with age: a retrospective review with susceptibility-weighted MR imaging. Am. J. Neuroradiol. 29 (1), 176–183. [PubMed: 17989376]

Hare D, Ayton S, Bush A, Lei P, 2013. A delicate balance: iron metabolism and diseases of the brain. Front. Aging Neurosci. 5, 34. [PubMed: 23874300]

Haris M, McArdle E, Fenty M, Singh A, Davatzikos C, Trojanowski JQ, et al., 2009. Early marker for Alzheimer's disease: hippocampus T1rho (T(1ρ)) estimation. J. Magnet. Resonance Imag. 29 (5), 1008–1012.

Heath F, Hurley SA, Johansen-Berg H, Sampaio-Baptista C, 2018. Advances in non-invasive myelin imaging. Dev Neurobiol78 (2), 136–151. [PubMed: 29082667]

Heidari M, Johnstone DM, Bassett B, Graham RM, Chua ACG, House MJ, et al., 2016. Brain iron accumulation affects myelin-related molecular systems implicated in a rare neurogenetic disease family with neuropsychiatric features. Mol. Psychiatry21 (11), 1599–1607. [PubMed: 26728570]

Jenkinson M, Beckmann CF, Behrens TE, Woolrich MW, Smith SM, 2012. FSL. Neuroimage62 (2), 782–790. [PubMed: 21979382]

Jones CK, Whittall KP, MacKay AL, 2003. Robust myelin water quantification: averaging vs. spatial filtering. Magn. Reson. Med. 50 (1), 206–209. [PubMed: 12815697]

Kabani NJ, Sled JG, Chertkow H, 2002. Magnetization transfer ratio in mild cognitive impairment and dementia of Alzheimer's type. Neuroimage15 (3), 604–610. [PubMed: 11848703]

Kalantari S, Laule C, Bjarnason TA, Vavasour IM, MacKay AL, 2011. Insight into in vivo magnetization exchange in human white matter regions. Magn. Reson. Med. 66 (4), 1142–1151. [PubMed: 21381107]

Keuken MC, Bazin PL, Backhouse K, Beekhuizen S, Himmer L, Kandola A, et al., 2017. Effects of aging on T_1, $T2^*$, and QSM MRI values in the subcortex. Brain Struct. Funct. 222 (6), 2487–2505. [PubMed: 28168364]

Killiany RJ, DeVivo R, Ellison A, Zhao Y, Steinberg E, Alosco ML, et al., 2020. Quantitative susceptibility mapping MRI reveals a relationship between iron accumulation, CDR score and cognition across the spectrum from healthy aging to Alzheimer's disease. Alzheimer's Dementia16 (S4), e044019.

Kirilina E, Helbling S, Morawski M, Pine K, Reimann K, Jankuhn S, et al., 2020. Superficial white matter imaging: contrast mechanisms and whole-brain in vivo mapping. Sci. Adv. 6 (41), eaaz9281.

Kolind S, Matthews L, Johansen-Berg H, Leite MI, Williams SC, Deoni S, et al., 2012. Myelin water imaging reflects clinical variability in multiple sclerosis. Neuroimage60 (1), 263–270. [PubMed: 22155325]

Kolind S, Seddigh A, Combes A, Russell-Schulz B, Tam R, Yogendrakumar V, et al., 2015. Brain and cord myelin water imaging: a progressive multiple sclerosis biomarker. NeuroImage Clin. 9, 574–580. [PubMed: 26594633]

Kor D, Birkl C, Ropele S, Doucette J, Xu T, Wiggermann V, et al., 2019. The role of iron and myelin in orientation dependent $R2^*$ of white matter. NMR Biomed. 32 (7), e4092. [PubMed: 31038240]

Kozlowski P, Liu J, Yung AC, Tetzlaff W, 2008. High-resolution myelin water measurements in rat spinal cord. Magn. Reson. Med. 59 (4), 796–802. [PubMed: 18302247]

Lane DJR, Ayton S, Bush AI, 2018. Iron and Alzheimer's Disease: an Update on Emerging Mechanisms. J. Alzheimer's Dis. 64 (s1), S379–Ss95. [PubMed: 29865061]

Langkammer C, Schweser F, Krebs N, Deistung A, Goessler W, Scheurer E, et al., 2012. Quantitative susceptibility mapping (QSM) as a means to measure brain iron? A post mortem validation study. Neuroimage62 (3), 1593–1599. [PubMed: 22634862]

Laule C, Kozlowski P, Leung E, Li DK, Mackay AL, Moore GR, 2008. Myelin water imaging of multiple sclerosis at 7 T: correlations with histopathology. Neuroimage40 (4), 1575–1580. [PubMed: 18321730]

Laule C, Leung E, Lis DK, Traboulsee AL, Paty DW, MacKay AL, et al., 2006. Myelin water imaging in multiple sclerosis: quantitative correlations with histopathology. Mult. Scler. 12 (6), 747–753. [PubMed: 17263002]

Lazari A, Lipp I, 2021. Can MRI measure myelin? Systematic review, qualitative assessment, and meta-analysis of studies validating microstructural imaging with myelin histology. Neuroimage, 117744.

Le Bihan D, Turner R, MacFall JR, 1989. Effects of intravoxel incoherent motions (IVIM) in steady-state free precession (SSFP) imaging: application to molecular diffusion imaging. Magn. Reson. Med. 10 (3), 324–337. [PubMed: 2733589]

Lee J, Hyun J−W, Lee J, Choi E−J, Shin H−G, Min K, et al., 2021. So you want to image myelin using MRI: an overview and practical guide for myelin water imaging. J. Magn. Reson. Imaging53 (2), 360–373. [PubMed: 32009271]

Lee J, Shmueli K, Fukunaga M, van Gelderen P, Merkle H, Silva AC, et al., 2010. Sensitivity of MRI resonance frequency to the orientation of brain tissue microstructure. Proc. Natl. Acad. Sci. 107 (11), 5130–5135. [PubMed: 20202922]

Lee J, Shmueli K, Kang BT, Yao B, Fukunaga M, van Gelderen P, et al., 2012. The contribution of myelin to magnetic susceptibility-weighted contrasts in high-field MRI of the brain. Neuroimage59 (4), 3967–3975. [PubMed: 22056461]

Levesque IR, Chia CL, Pike GB, 2010. Reproducibility of in vivo magnetic resonance imaging-based measurement of myelin water. J. Magnet. Resonance Imag. 32 (1), 60–68.

Li W, Wu B, Liu C, 2011. Quantitative susceptibility mapping of human brain reflects spatial variation in tissue composition. Neuroimage55 (4), 1645–1656. [PubMed: 21224002]

Li Y, Sethi SK, Zhang C, Miao Y, Yerramsetty KK, Palutla VK, et al., 2021. Iron content in deep gray matter as a function of age using quantitative susceptibility mapping: a multicenter study. Front. Neurosci. 14 (1389).

Lin PY, Chao TC, Wu ML, 2015. Quantitative susceptibility mapping of human brain at 3T: a multisite reproducibility study. AJNR Am. J. Neuroradiol. 36 (3), 467–474. [PubMed: 25339652]

Liu C, Li W, Tong KA, Yeom KW, Kuzminski S, 2015a. Susceptibility-weighted imaging and quantitative susceptibility mapping in the brain. J. Magnet. Resonance Imag. 42 (1), 23–41.

Liu C, Li W, Tong KA, Yeom KW, Kuzminski S, 2015b. Susceptibility-weighted imaging and quantitative susceptibility mapping in the brain. J. Magnet. Resonance Imag. 42 (1), 23–41.

Liu C, 2010. Susceptibility tensor imaging. Magn. Reson. Med. 63 (6), 1471–1477. [PubMed: 20512849]

Loeffer DA, Connor JR, Juneau PL, Snyder BS, Kanaley L, DeMaggio AJ, et al., 1995. Transferrin and Iron in Normal, Alzheimer's Disease, and Parkinson's Disease Brain Regions. J. Neurochem. 65 (2), 710–716. [PubMed: 7616227]

MacKay A, Whittall K, Adler J, Li D, Paty D, Graeb D, 1994. In vivo visualization of myelin water in brain by magnetic resonance. Magn. Reson. Med. 31 (6), 673–677. [PubMed: 8057820]

MacKay AL, Laule C, 2016. Magnetic Resonance of Myelin Water: an in vivo Marker for Myelin. Brain Plast2 (1), 71–91. [PubMed: 29765849]

McCreary CR, Bjarnason TA, Skihar V, Mitchell JR, Yong VW, Dunn JF, 2009. Multiexponential T2 and magnetization transfer MRI of demyelination and remyelination in murine spinal cord. Neuroimage45 (4), 1173–1182. [PubMed: 19349232]

Meadowcroft MD, Wang J, Purnell CJ, Peters DG, Eslinger PJ, Neely EB, et al., 2016. Reduced white matter MRI transverse relaxation rate in cognitively normal H63D-HFE human carriers and H67D-HFE mice. Brain Imaging Behav. 10 (4), 1231–1242. [PubMed: 26660104]

Mills E, Dong X−P, Wang F, Xu H, 2010. Mechanisms of brain iron transport: insight into neurodegeneration and CNS disorders. Future Med. Chem. 2 (1), 51–64. [PubMed: 20161623]

Möller HE, Bossoni L, Connor JR, Crichton RR, Does MD, Ward RJ, et al., 2019. Iron, Myelin, and the Brain: neuroimaging Meets Neurobiology. Trends Neurosci..

Myint W, Ishima R, 2009. Chemical exchange effects during refocusing pulses in constant-time CPMG relaxation dispersion experiments. J. Biomol. NMR45 (1–2), 207–216. [PubMed: 19618276]

Nasrabady SE, Rizvi B, Goldman JE, Brickman AM, 2018a. White matter changes in Alzheimer's disease: a focus on myelin and oligodendrocytes. Acta Neuropathol Commun6, 22. [PubMed: 29499767]

Nasrabady SE, Rizvi B, Goldman JE, Brickman AM, 2018b. White matter changes in Alzheimer's disease: a focus on myelin and oligodendrocytes. Acta Neuropathol Commun6 (1), 22. [PubMed: 29499767]

Ogg RJ, Langston JW, Haacke EM, Steen RG, Taylor JS, 1999. The correlation between phase shifts in gradient-echo MR images and regional brain iron concentration. Magn Reson Imaging17 (8), 1141–1148. [PubMed: 10499676]

Okubo G, Okada T, Yamamoto A, Fushimi Y, Okada T, Murata K, et al., 2017. Relationship between aging and T1 relaxation time in deep gray matter: a voxel-based analysis. J. Magnet. Resonance Imag. 46 (3), 724–731.

Ortiz E, Pasquini JM, Thompson K, Felt B, Butkus G, Beard J, et al., 2004. Effect of manipulation of iron storage, transport, or availability on myelin composition and brain iron content in three different animal models. J. Neurosci. Res. 77 (5), 681–689. [PubMed: 15352214]

Papadaki E, Kavroulakis E, Kalaitzakis G, Karageorgou D, Makrakis D, Maris TG, et al., 2019. Age-related deep white matter changes in myelin and water content: a T2 relaxometry study. J. Magn. Reson. Imaging50 (5), 1393–1404. [PubMed: 30859698]

Persson N, Wu J, Zhang Q, Liu T, Shen J, Bao R, et al., 2015. Age and sex related differences in subcortical brain iron concentrations among healthy adults. Neuroimage122, 385–398. [PubMed: 26216277]

Peters A, 2002. The effects of normal aging on myelin and nerve fibers: a review. J. Neurocytol. 31 (8–9), 581–593. [PubMed: 14501200]

Pfefferbaum A, Adalsteinsson E, Rohlfing T, Sullivan EV, 2009. MRI estimates of brain iron concentration in normal aging: comparison of field-dependent (FDRI) and phase (SWI) methods. Neuroimage47 (2), 493–500. [PubMed: 19442747]

Piredda GF, Hilbert T, Thiran J−P, Kober TProbing myelin content of the human brain with MRI: a review. Magnetic resonance in medicine.n/a(n/a)2021.

Prasloski T, Madler B, Xiang QS, MacKay A, Jones C, 2012. Applications of stimulated echo correction to multicomponent T2 analysis. Magn. Reson. Med. 67 (6), 1803–1814. [PubMed: 22012743]

Pu R, Wu Z, Yu W, He H, Zhou Z, Wang Z, et al., 2020. The association of myelination in the internal capsule with iron deposition in the basal ganglia in macaques: a magnetic resonance imaging study. Quant. Imaging Med. Surg. 10 (7), 1526–1539. [PubMed: 32676370]

Qian W, Khattar N, Cortina LE, Spencer RG, Bouhrara M, 2020. Nonlinear associations of neurite density and myelin content with age revealed using multicomponent diffusion and relaxometry magnetic resonance imaging. Neuroimage223, 117369. [PubMed: 32931942]

Ramos P, Santos A, Pinto NR, Mendes R, Magalhaes T, Almeida A, 2014. Iron levels in the human brain: a post-mortem study of anatomical region differences and age-related changes. J. Trace Elements Med. Biol. 28 (1), 13–17.

Schonberg DL, Goldstein EZ, Sahinkaya FR, Wei P, Popovich PG, McTigue DM, 2012. Ferritin stimulates oligodendrocyte genesis in the adult spinal cord and can be transferred from macrophages to NG2 cells in vivo. J. Neurosci.J. Neurosci. 32 (16), 5374–5384. [PubMed: 22514302]

Schonberg DL, McTigue DM, 2009. Iron is essential for oligodendrocyte genesis following intraspinal macrophage activation. Exp. Neurol. 218 (1), 64–74. [PubMed: 19374902]

Sehgal V, Delproposto Z, Haacke EM, Tong KA, Wycliffe N, Kido DK, et al., 2005. Clinical applications of neuroimaging with susceptibility-weighted imaging. J. Magnet. Resonance Imag. 22 (4), 439–450.

Seland JG, Washburn KE, Anthonsen HW, Krane J, 2004. Correlations between diffusion, internal magnetic field gradients, and transverse relaxation in porous systems containing oil and water. Phys. Rev. E, Statistical, Nonlinear, Soft Matter Physics70 (5 Pt 1), 051305.

Shock N, 1985. Normal Human Aging: the Baltimore Longitudinal Study of Aging. J Gerontol40 (6), 767–774.

Sirrs SM, Laule C, Madler B, Brief EE, Tahir SA, Bishop C, et al., 2007. Normal-appearing white matter in patients with phenylketonuria: water content, myelin water fraction, and metabolite concentrations. Radiology242 (1), 236–243. [PubMed: 17185670]

Slater DA, Melie-Garcia L, Preisig M, Kherif F, Lutti A, Draganski B, 2019. Evolution of white matter tract microstructure across the life span. Hum Brain Mapp40 (7), 2252–2268. [PubMed: 30673158]

Smith SM, 2002. Fast robust automated brain extraction. Hum Brain Mapp17 (3), 143–155. [PubMed: 12391568]

Stankiewicz JM, Neema M, Ceccarelli A, 2014. Iron and multiple sclerosis. Neurobiol. Aging35, S51–SS8. [PubMed: 24929968]

Steiger TK, Weiskopf N, Bunzeck N, 2016. Iron Level and Myelin Content in the Ventral Striatum Predict Memory Performance in the Aging Brain. J. Neurosci.J. Neurosci. 36 (12), 3552–3558. [PubMed: 27013683]

Stollberger R, Wach P, 1996. Imaging of the active B1 field in vivo. Magn. Reson. Med. 35 (2), 246–251. [PubMed: 8622590]

Tang Y, Nyengaard JR, Pakkenberg B, Gundersen HJ, 1997. Age-induced white matter changes in the human brain: a stereological investigation. Neurobiol. Aging18 (6), 609–615. [PubMed: 9461058]

Todorich B, Pasquini JM, Garcia CI, Paez PM, Connor JR, 2009. Oligodendrocytes and myelination: the role of iron. Glia57 (5), 467–478. [PubMed: 18837051]

Uddin MN, Figley TD, Solar KG, Shatil AS, Figley CR, 2019. Comparisons between multi-component myelin water fraction, T1w/T2w ratio, and diffusion tensor imaging measures in healthy human brain structures. Sci Rep9 (1), 2500. [PubMed: 30792440]

van der Flier WM, van den Heuvel DM, Weverling-Rijnsburger AW, Bollen EL, Westendorp RG, van Buchem MA, et al., 2002. Magnetization transfer imaging in normal aging, mild cognitive impairment, and Alzheimer's disease. Ann. Neurol. 52 (1), 62–67. [PubMed: 12112048]

van der Weijden MCM, van Laar PJ, Lambrechts RA, Verbeek DS, Tijssen MAJ, 2019. Cortical pencil lining on SWI MRI in NBIA and healthy aging. BMC Neurol19 (1), 233. [PubMed: 31607263]

Vavasour IM, Clark CM, Li DK, Mackay AL, 2006. Reproducibility and reliability of MR measurements in white matter: clinical implications. Neuroimage32 (2), 637–642. [PubMed: 16677833]

Wang D, Li W−B, Wei X−E, Li Y−H, Dai Y−M, 2012. An Investigation of Age-Related Iron Deposition Using Susceptibility Weighted Imaging. PLoS ONE7 (11), e50706.

Wang Y, Liu T, 2015. Quantitative susceptibility mapping (QSM): decoding MRI data for a tissue magnetic biomarker. Magn. Reson. Med. 73 (1), 82–101. [PubMed: 25044035]

Ward RJ, Zucca FA, Duyn JH, Crichton RR, Zecca L, 2014. The role of iron in brain ageing and neurodegenerative disorders. Lancet Neurol. 13 (10), 1045–1060. [PubMed: 25231526]

Washburn KE, Eccles CD, Callaghan PT, 2008. The dependence on magnetic field strength of correlated internal gradient relaxation time distributions in heterogeneous materials. J. Magnetic Resonance (San Diego, Calif: 1997)194 (1), 33–40.

Webb S, Munro CA, Midha R, Stanisz GJ, 2003. Is multicomponent T2 a good measure of myelin content in peripheral nerve?Magn. Reson. Med. 49 (4), 638–645. [PubMed: 12652534]

West DJ, Teixeira RPAG, Wood TC, Hajnal JV, Tournier J−D, Malik SJ, 2019. Inherent and unpredictable bias in multi-component DESPOT myelin water fraction estimation. Neuroimage195, 78–88. [PubMed: 30930311]

Westlye LT, Walhovd KB, Dale AM, Bjornerud A, Due-Tonnessen P, Engvig A, et al., 2010. Life-span changes of the human brain white matter: diffusion tensor imaging (DTI) and volumetry. Cerebral Cortex (New York, NY: 1991)20 (9), 2055–2068.

Whittall KP, MacKay AL, Graeb DA, Nugent RA, Li DK, Paty DW, 1997. In vivo measurement of T2 distributions and water contents in normal human brain. Magn. Reson. Med. 37 (1), 34–43. [PubMed: 8978630]

Xu X, Wang Q, Zhang M, 2008. Age, gender, and hemispheric differences in iron deposition in the human brain: an in vivo MRI study. Neuroimage40 (1), 35–42. [PubMed: 18180169]

Yao B, Li TQ, Gelderen P, Shmueli K, de Zwart JA, Duyn JH, 2009. Susceptibility contrast in high field MRI of human brain as a function of tissue iron content. Neuroimage44 (4), 1259–1266. [PubMed: 19027861]

Yao Y, Nguyen TD, Pandya S, Zhang Y, Hurtado Rúa S, Kovanlikaya I, et al., 2018. Combining Quantitative Susceptibility Mapping with Automatic Zero Reference (QSM0) and Myelin Water Fraction Imaging to Quantify Iron-Related Myelin Damage in Chronic Active MS Lesions. AJNR Am. J. Neuroradiol. 39 (2), 303–310. [PubMed: 29242359]

Yeatman JD, Wandell BA, Mezer AA, 2014. Lifespan maturation and degeneration of human brain white matter. Nat Commun. 5, 4932. [PubMed: 25230200]

Zhang J, Kolind SH, Laule C, MacKay AL, 2015a. How does magnetization transfer influence mcDESPOT results?Magn. Reson. Med. 74 (5), 1327–1335. [PubMed: 25399771]

Zhang J, Kolind SH, Laule C, MacKay AL, 2015b. Comparison of myelin water fraction from multiecho T2 decay curve and steady-state methods. Magn. Reson. Med. 73 (1), 223–232. [PubMed: 24515972]

Zhang Y, Wei H, Cronin MJ, He N, Yan F, Liu C, 2018. Longitudinal data for magnetic susceptibility of normative human brain development and aging over the lifespan. Data Brief20, 623–631. [PubMed: 30197920]

Ziener CH, Kampf T, Jakob PM, Bauer WR, 2010. Diffusion effects on the CPMG relaxation rate in a dipolar field. J. Magnetic Resonance (San Diego, Calif: 1997)202 (1), 38–42.

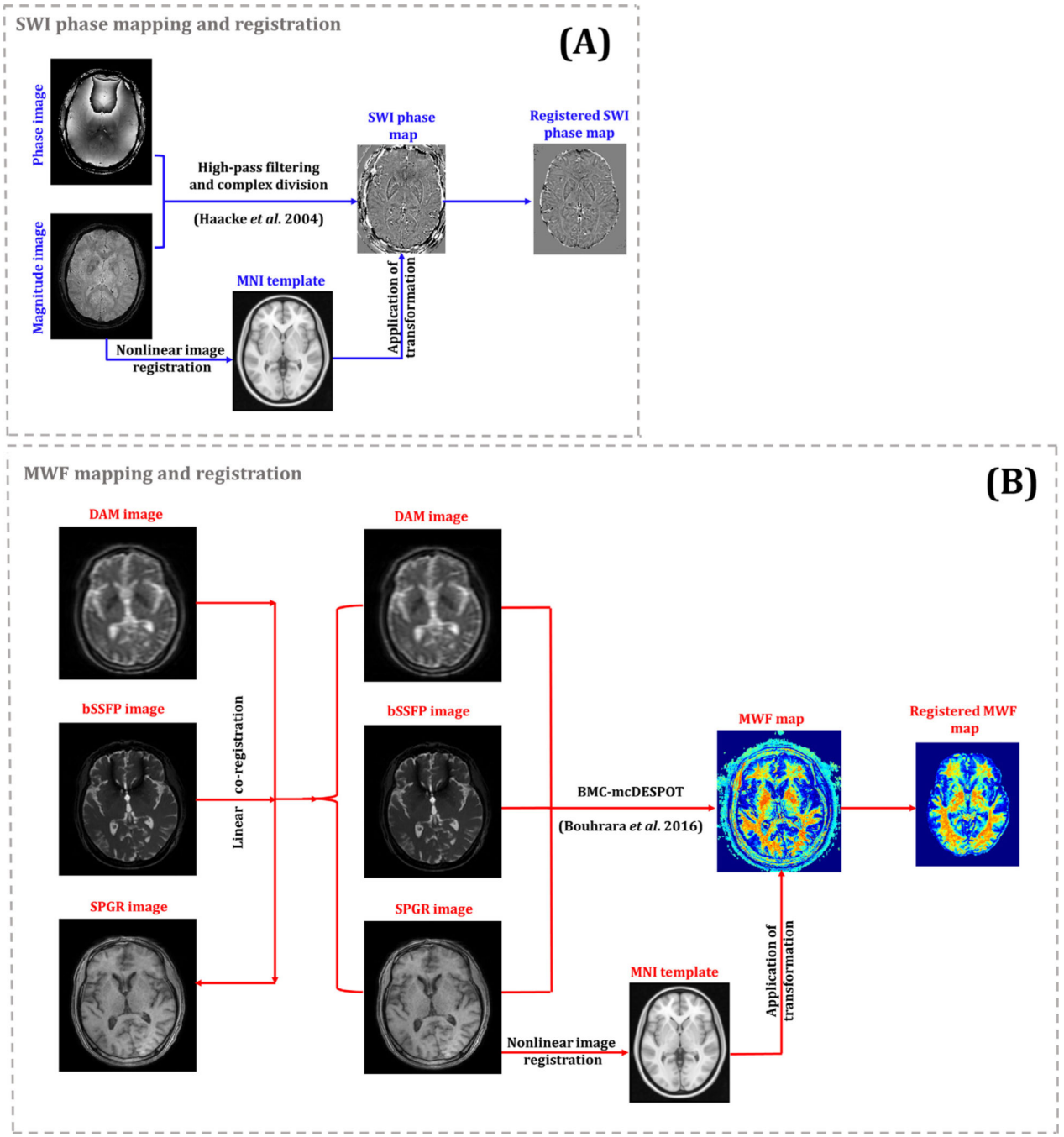

Fig. 1.
Diagram of the A) SWI phase mapping and B) MWF mapping, and registration workflow.

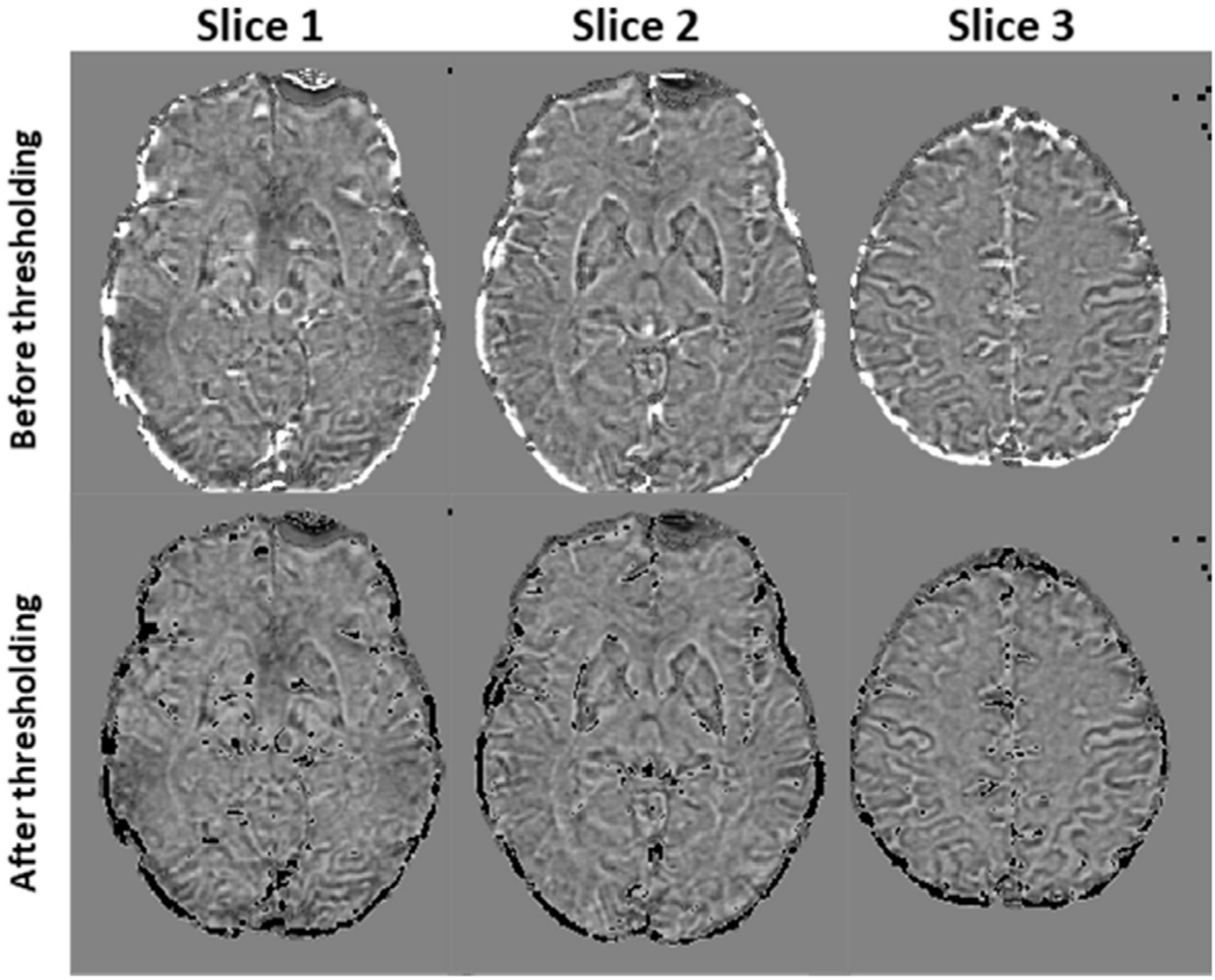

Fig. 2.

Examples of SWI phase maps before (original) and after signal thresholding. A threshold was applied to discard abnormally high phase values seen in areas with strong magnetic susceptibility or high iron concentration. Black voxels represent the discarded areas. Results are shown for three different slices.

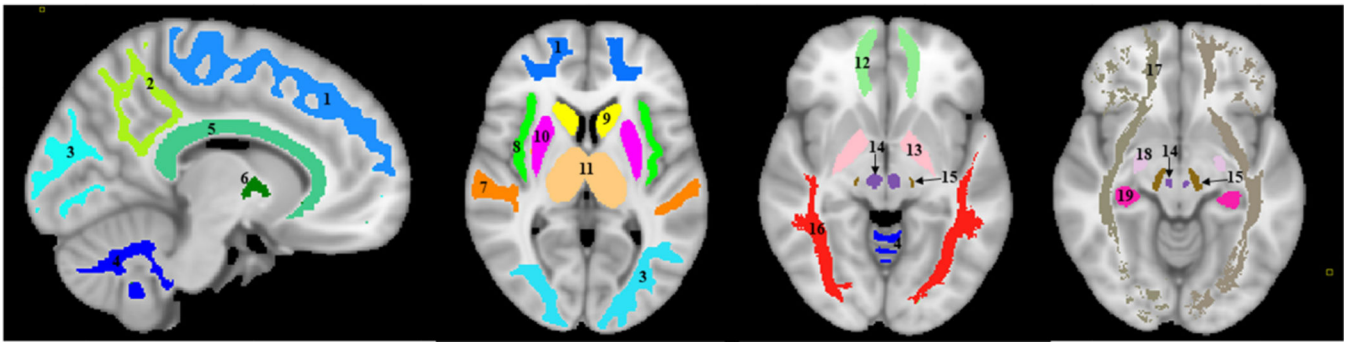

Fig. 3.

Visualization of the white matter and deep gray matter ROIs investigated in our analysis. 1) Frontal lobes, 2) Parietal lobes, 3) Occipital lobes, 4) Cerebellum, 5) Corpus callosum, 6) Internal capsules, 7) Temporal lobes, 8) Insula, 9) Caudate, 10) Putamen, 11) Thalamus, 12) Forceps, 13) Globus pallidus, 14) Red nucleus, 15) Substantia nigra, 16) Longitudinal fasciculus, 17) Fronto-occipital fasciculus, 18) Amygdala, and 19) Hippocampus.

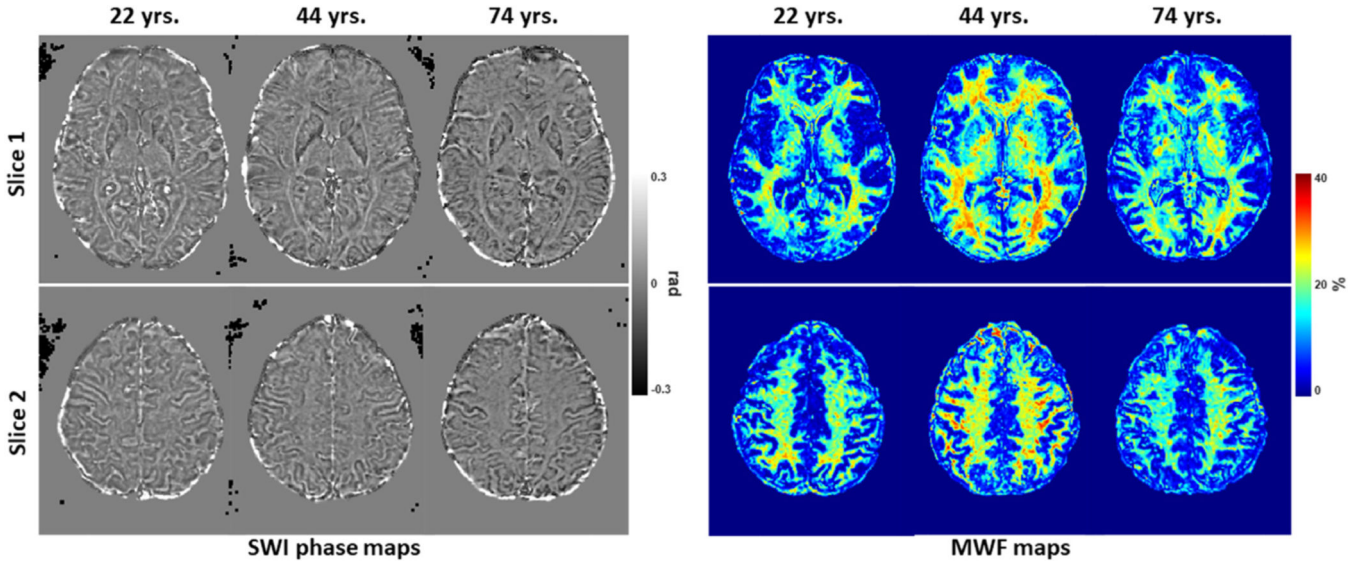

Fig. 4.

SWI phase and MWF maps derived from the brains of three men participants of different ages. For each participant, results are shown for two representative slices.

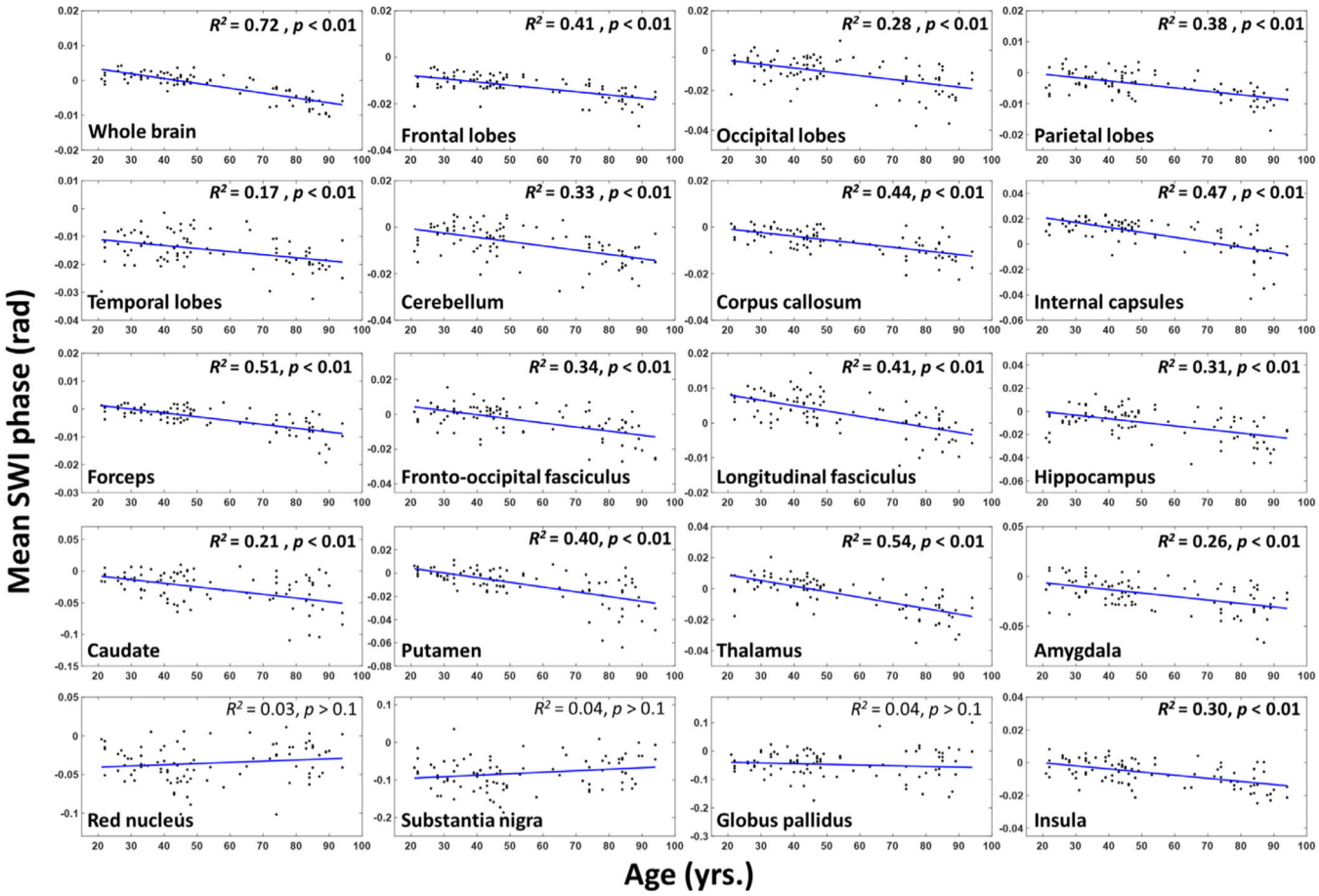

Fig. 5.

Regressions of SWI phase with age ($N = 92$). Results are shown for twenty WM and DGM brain structures. The coefficient of determination, R^2, and the significance, p-value (FDR corrected), of the multiple linear regression model are as shown. Most ROIs exhibited significant negative correlations between SWI phase, that is, positive correlations between iron content, and age.

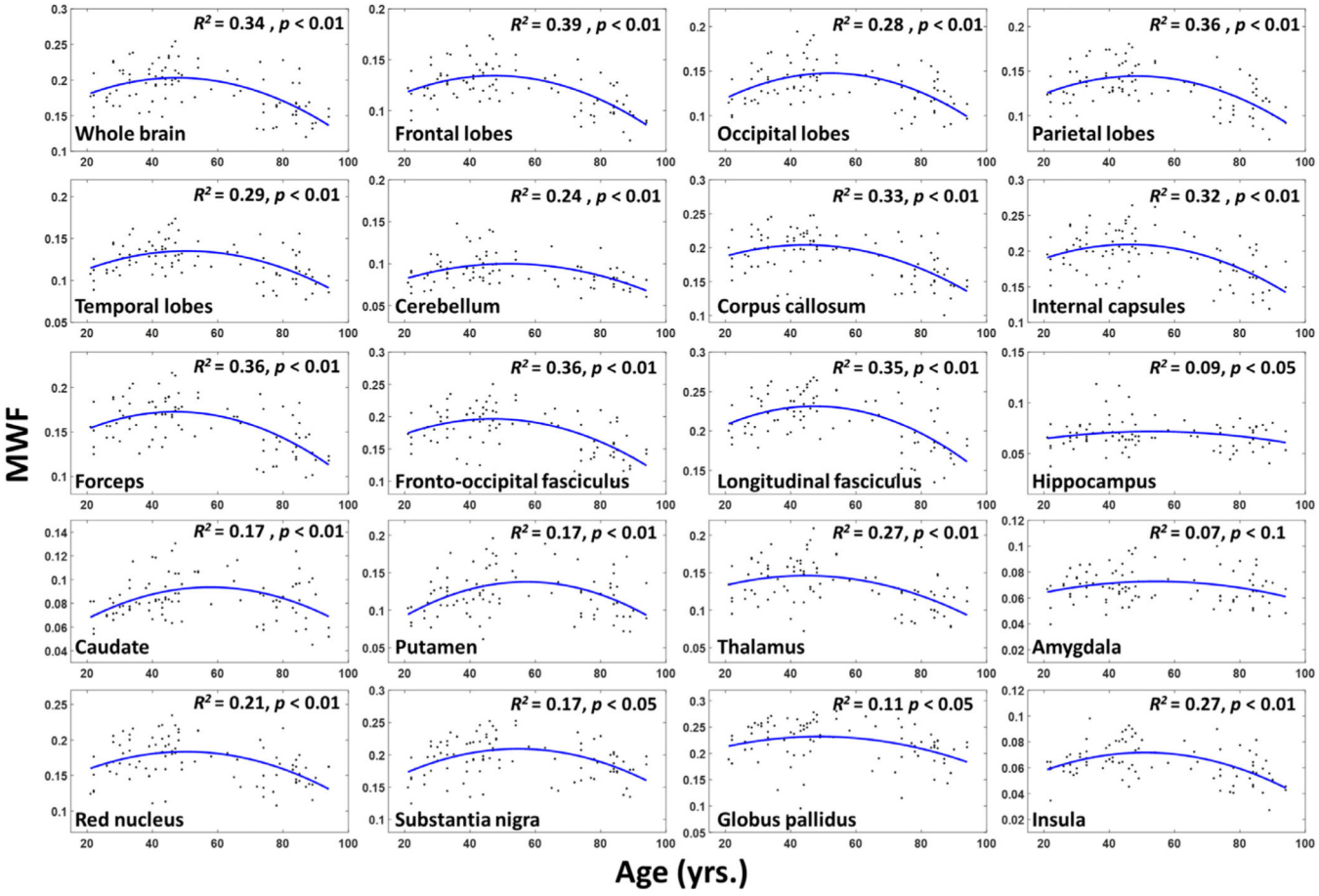

Fig. 6.

Regional myelin water fraction (MWF) trends as a function of age ($N = 92$). Results are shown for twenty WM and DGM brain structures. For each ROI, the coefficient of determination, $R^{2,}$ and the significance, p-value (FDR corrected), of the multiple linear regression model are as shown. All regions investigated show significant inverted U-shaped trends of MWF with age, with differences in detail between regions.

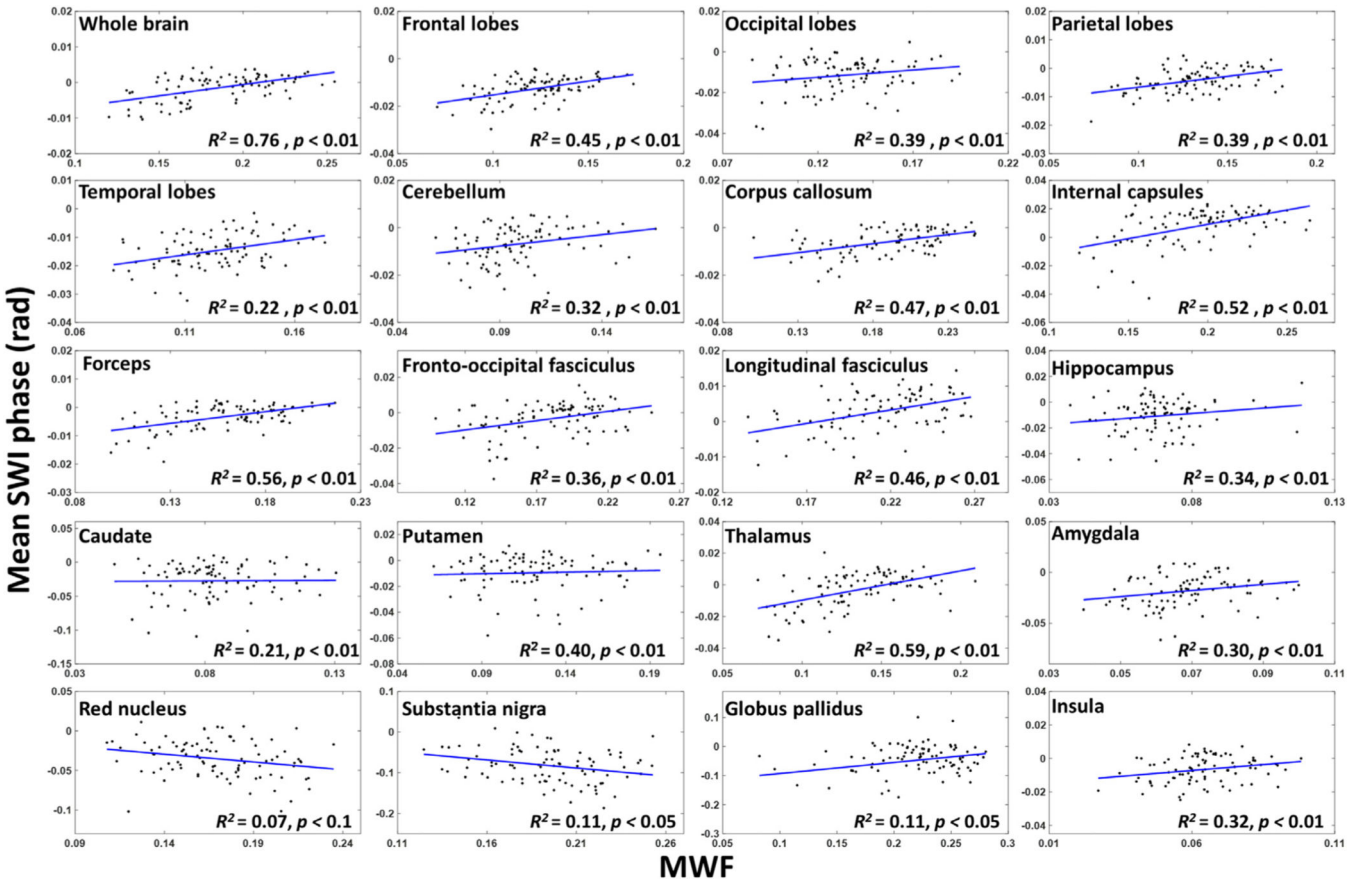

Fig. 7.

Regressions of SWI phase with MWF (N = 92) adjusted for age and sex. Results are shown for twenty WM and DGM brain structures. The coefficient of determination, $R^{2,}$ and the significance, p-value, of the multiple linear regression model are as shown. All ROIs exhibited significant positive correlations between SWI phase and MWF indicating that lower MWF corresponds to lower SWI phase, that is, higher iron content.

Table 1

Slope, β, and significance, p, of the regression terms incorporated in the multiple linear regression given by: SWI phase $\sim \beta_0 + \beta_{age} \times$ age $+ \beta_{sex} \times$ sex. All p-values presented are obtained after FDR correction. Underlined p-values indicate close to significance before FDR correction.

	SWI phase			
	Age		**Sex**	
	β_{age} **(× 10^{-4})**	p_{age}	β_{sex}**(× 10^{-3})**	p_{sex}
WB	−1.39	< **0.01**	−0.27	> 0.1
FL	−1.40	< **0.01**	0.32	> 0.1
OL	−1.93	< **0.01**	0.28	> 0.1
PL	−1.10	< **0.01**	−0.85	> 0.1
TL	−1.09	< **0.01**	−0.14	> 0.1
CRB	−1.81	< **0.01**	−1.19	> 0.1
CC	−1.58	< **0.01**	−2.15	> 0.1
IC	−3.86	< **0.01**	−2.31	> 0.1
FOR	−1.37	< **0.01**	−1.39	> 0.1
FOF	−2.31	< **0.01**	−3.10	≥ 0.1
LF	−1.55	< **0.01**	0.08	> 0.1
Hip	−3.03	< **0.01**	−4.13	≥ 0.1
CN	−5.66	> 0.1	−7.76	> 0.1
Put	−4.09	> 0.1	1.18	> 0.1
Th	−3.59	< **0.01**	−1.25	> 0.1
Am	−3.45	< **0.01**	−1.86	> 0.1
RN	1.43	> 0.1	4.75	> 0.1
SN	3.88	< **0.1**	3.99	> 0.1
GP	−2.86	> 0.1	23.56	≥ 0.1
Ins	−1.89	< **0.01**	−0.56	> 0.1

SWI: susceptibility weighted imaging, WB: whole brain, FL: frontal lobes, PL: parietal lobes, TL: temporal lobes, OL: occipital lobes, CRB: cerebellum, CC: corpus callosum, IC: internal capsules, FOR: forceps, FOF: fronto-occipital fasciculus, LF: longitudinal fasciculus, Hip: hippocampus, CN: caudate nucleus, Put: putamen, Th: thalamus, Am: amygdala, RN: red nucleus, SN: substantia nigra, GP: globus pallidus, Ins: insula. Bold indicates significance (p <.05) or close to significance (p <.1).

Table 2

Slope, β, and significance, p, of the regression terms incorporated in the multiple linear regression given by: MWF $\sim \beta_0 + \beta_{age} \times \text{age} + \beta_{age^2} \times \text{age}^2 + \beta_{sex} \times \text{sex}$. All p-values presented are obtained after FDR correction. Underlined p-values indicate close to significance before FDR correction.

	MWF					
	Age		**Age^2**		**Sex**	
	$\beta_{age}(\times 10^{-4})$	p_{age}	$\beta_{age^2}(\times 10^{-5})$	p_{age^2}	$\beta_{sex}(\times 10^{-3})$	p_{sex}
WB	− 3.93	< **0.01**	− 3.12	< **0.01**	1.32	> 0.1
FL	− 2.87	< **0.01**	− 2.26	< **0.01**	1.06	> 0.1
OL	− 1.01	< **0.01**	− 2.77	< **0.01**	0.26	> 0.1
PL	− 2.75	< **0.01**	− 2.47	< **0.01**	− 1.13	> 0.1
TL	− 1.58	< **0.01**	− 2.33	< **0.01**	0.41	> 0.1
CRB	− 0.79	< **0.01**	− 1.92	< **0.01**	5.74	> 0.1
CC	− 5.22	< **0.01**	− 2.73	< **0.01**	− 2.52	> 0.1
IC	− 4.57	< **0.01**	− 2.96	< **0.01**	2.03	> 0.1
FOR	− 3.73	< **0.01**	− 2.74	< **0.01**	1.18	> 0.1
FOF	− 4.57	< **0.01**	− 3.36	< **0.01**	4.57	> 0.1
LF	− 4.28	< **0.01**	− 3.29	< **0.01**	2.93	> 0.1
Hip	− 0.12	> 0.1	− 0.80	< **0.05**	6.39	≥ 0.1
CN	− 1.42	> 0.1	− 1.95	< **0.01**	3.59	> 0.1
Put	− 2.21	> 0.1	− 3.43	< **0.01**	6.41	> 0.1
Th	− 4.03	< **0.01**	− 2.32	< **0.01**	8.14	> 0.1
Am	0.04	> 0.1	− 0.81	< **0.05**	2.91	> 0.1
RN	− 2.01	< **0.01**	− 2.72	< **0.01**	− 0.90	> 0.1
SN	0.48	> 0.1	− 3.16	< **0.01**	− 0.06	> 0.1
GP	− 2.42	< **0.05**	− 2.33	< **0.05**	− 1.27	> 0.1
Ins	− 0.89	< **0.01**	− 1.54	< **0.01**	2.50	> 0.1

MWF: myelin water fraction, WB: whole brain, FL: frontal lobes, PL: parietal lobes, TL: temporal lobes, OL: occipital lobes, CRB: cerebellum, CC: corpus callosum, IC: internal capsules, FOR: forceps, FOF: fronto-occipital fasciculus, LF: longitudinal fasciculus, Hip: hippocampus, CN: caudate nucleus, Put: putamen, Th: thalamus, Am: amygdala, RN: red nucleus, SN: substantia nigra, GP: globus pallidus, Ins: insula. Bold indicates significance (p <.05) or close to significance (p <.1).

Table 3

Slope, β, and significance, p, of the regression terms incorporated in the multiple linear regression given by: SWI $\sim \beta_0 + \beta_{age} \times$ age $+ \beta_{MWF} \times$ MWF $+ \beta_{sex} \times$ sex. All p-values presented are obtained after FDR correction. Underlined p-values indicate close-to-significance before FDR correction and double-underlined p-values indicate significance before FDR correction.

	SWI phase					
	Age		**MWF**		**Sex**	
β_{age} ($\times 10^{-4}$)	p_{age}	β_{MWF}($\times 10^{-2}$)	p_{MWF}	β_{sex}($\times 10^{-3}$)	p_{sex}	
WB	− 1.23	< **0.01**	2.44	< **0.05**	− 0.21	> 0.1
FL	− 1.13	< **0.01**	5.96	< **0.05**	0.42	> 0.1
OL	− 1.86	< **0.01**	2.03	> 0.1	0.35	> 0.1
PL	− 0.93	< **0.01**	3.58	< **0.05**	− 0.70	> 0.1
TL	− 0.84	< **0.01**	7.55	< **0.05**	− 0.04	> 0.1
CRB	− 1.78	< **0.01**	1.39	> 0.1	− 1.24	> 0.1
CC	− 1.34	< **0.01**	3.32	< **0.05**	− 0.02	> 0.1
IC	− 3.19	< **0.01**	10.10	< **0.05**	− 2.17	> 0.1
FOR	− 1.16	< **0.01**	3.76	< **0.05**	− 0.06	> 0.1
FOF	− 2.04	< **0.01**	3.94	> 0.1	− 3.12	≥ 0.1
LF	− 1.31	< **0.01**	3.51	< **0.05**	− 0.11	> 0.1
Hip	− 2.92	< **0.01**	15.74	< **0.1**	− 5.00	> 0.1
CN	− 5.66	> 0.1	2.62	> 0.1	− 0.08	> 0.1
Put	− 4.09	> 0.1	1.84	> 0.1	1.14	> 0.1
Th	− 3.07	< **0.01**	9.17	< **0.05**	− 1.75	> 0.1
Am	− 3.32	< **0.01**	25.25	< **0.05**	− 2.18	> 0.1
RN	0.74	> 0.1	− 17.39	< **0.1**	4.04	> 0.1
SN	3.22	≥ 0.1	− 36.00	< **0.05**	2.62	> 0.1
GP	− 1.15	> 0.1	39.25	< **0.05**	25.57	> 0.1
Ins	− 1.77	< **0.01**	5.13	> 0.1	− 0.04	> 0.1

SWI: susceptibility weighted imaging, WB: whole brain, FL: frontal lobes, PL: parietal lobes, TL: temporal lobes, OL: occipital lobes, CRB: cerebellum, CC: corpus callosum, IC: internal capsules, FOR: forceps, FOF: fronto-occipital fasciculus, LF: longitudinal fasciculus, Hip: hippocampus, CN: caudate nucleus, Put: putamen, Th: thalamus, Am: amygdala, RN: red nucleus, SN: substantia nigra, GP: globus pallidus, Ins: insula. Bold indicates significance (p <.05) or close to significance (p <.1).